

FL7 is an ancient ABA-independent inhibitor of PP2C-As regulating plant stress responses

Received: 5 June 2024

Accepted: 30 October 2025

Published online: 15 December 2025

 Check for updates

Tianli Li  ^{1,2,11}, Zitong Yang  ^{1,2,11}, Guojun Li ^{3,4,5}, Jan de Vries  ^{6,7,8}, Yuke Li ^{1,2}, Xianglan Li ^{1,2}, Xu Lu ^{1,2}, Xinyi Gu ^{1,2}, Zhaojie Chen ⁹, Yang Zhao  ^{3,4,5}, Daolong Dou  ^{1,2,10}, Danyu Shen  ^{1,2}  & Gan Ai  ^{1,2} 

Clade A protein phosphatase 2Cs (PP2C-As) play crucial roles in plant stress responses. Although the ABA receptors PYLs inhibit PP2C-As in an ABA-dependent manner, other modulators of these phosphatases remain largely unknown. Here, we identify the FORKED-LIKE 7 (FL7) protein as a broad PP2C-A interactor that effectively suppresses PP2C activity through an ABA-independent, noncompetitive mechanism. By inhibiting PP2C-A activity, FL7 positively regulates osmotic tolerance and plant immunity in an ABA-independent manner. The N-terminal auxin canalisation (AC) domain of FL7 is required for its PP2C-As inhibitory activity. Further evolutionary analyses reveal that FL7 homologues containing an AC domain belong to an ancient family that emerged in a common ancestor of Klebsormidiophyceae algae and land plants. Genetic analyses indicate that algal FL7 homologues have a conserved function as PP2C-A inhibitors. Our study reveals an ABA-independent layer of PP2C-A modulation that regulates biotic and abiotic stress responses, which is likely conserved across a billion years of streptophyte evolution and predated the PYL-ABA regulation established in the common ancestor of land plants.

Owing to the climate crisis, plants face ever-increasing soil salinization and periods of drought, imposing osmotic stresses that adversely affect crop growth, yield, and resistance to disease^{1,2}. High soil salinity, in particular, heightens plant vulnerability to soil-borne pathogens. For instance, irrigation with saline water significantly compromises onion resistance to *Fusarium oxysporum*³, while tomato and chrysanthemum grown in high-salinity nutrient solutions exhibit increased disease severity caused by *Phytophthora parasitica* or *P. cryptogea*⁴. This phenomenon is partially attributed to the accumulation of the phytohormone abscisic acid (ABA), which antagonizes salicylic acid (SA), a vital defence hormone, under osmotic stress conditions^{5,6}.

Consistently, ABA application induces disease susceptibility in different plants, such as *Arabidopsis thaliana*, tomato, and soybean, independent of the pathogen's lifestyle^{7,8}. These findings highlight the crosstalk between plant osmotic stress and defence responses; however, the underlying mechanisms remain largely elusive, posing a considerable challenge to the development of climate-resilient crop varieties.

During evolution, intricate signalling mechanisms have emerged through which plants exhibit appropriate responses to withstand osmotic and pathogenic stress⁹. Central to these stress response pathways is the reversible phosphorylation of proteins, facilitated by

¹State Key Laboratory of Agricultural and Forestry Biosecurity, Nanjing Agricultural University, Nanjing, China. ²College of Plant Protection, Nanjing Agricultural University, Nanjing, China. ³CAS Center for Excellence in Molecular Plant Sciences, The Chinese Academy of Sciences, Shanghai, China. ⁴Key Laboratory of Plant Carbon Capture, The Chinese Academy of Sciences, Shanghai, China. ⁵University of Chinese Academy of Sciences, Beijing, China.

⁶Department of Applied Bioinformatics, University of Goettingen, Goettingen, Germany. ⁷Campus Institute Data Science (CIDAS), University of Goettingen, Goettingen, Germany. ⁸Department of Applied Bioinformatics, Goettingen Center for Molecular Biosciences (GZMB), University of Goettingen, Goettingen, Germany. ⁹Guangxi Key Laboratory of Agric-Environment and Agric-Products Safety, College of Agriculture, Guangxi University, Nanning, Guangxi, China. ¹⁰Academy for Advanced Interdisciplinary Studies, Nanjing Agricultural University, Nanjing, China. ¹¹These authors contributed equally: Tianli Li, Zitong Yang.  e-mail: shendanyu@njau.edu.cn; ganai@njau.edu.cn

the coordinated actions of protein kinases and protein phosphatases¹⁰. In particular, the clade A protein phosphatase 2 C (PP2C-A) family plays a pivotal role in regulating plant stress signalling networks¹¹ and might act as a hub linking plant osmotic and defence responses. *Arabidopsis* encodes 9 PP2C-As, including ABA INSENSITIVE 1/2 (ABI1/2), HYPER-SENSITIVE TO ABA1/2 (HAB1/2), HYPERSENSITIVE GERMINATION 1/3 (AHG1/3), and HIGHLY ABA-INDUCED1/2/3 (HAI1/2/3). All of the enzymes are functional phosphatases and negative regulators of the plant osmotic stress response^{12,13}. For example, *HAI1/2/3* single mutants exhibit increased proline and osmoregulatory solute accumulation at low water potential¹⁴, whereas *AHG1/3* or *ABI1/2* mutants exhibit increased drought tolerance¹⁵. PP2C-As also negatively regulate plant defence responses. HAI1 interacts with mitogen-activated protein kinases 3/6 (MPK3/6) and dephosphorylates them to suppress MPK3/6 activation, leading to weakened plant immunity¹⁶. ABI1 can also interact with and dephosphorylate MPK6¹⁷.

PP2C-As lack regulatory subunits^{18,19}; thus, their activities are precisely fine-tuned by those of other proteins. PYR/PYL/RCAR proteins (PYLs), which are important components of the ABA signalling pathway, are well known regulators of PP2C-As. In the absence of ABA, PP2C-As are associated with Snf1-related kinases 2 (SnRKs), including SnRK2.2/2.3/2.6, keeping them inactive by dephosphorylating their activation loops and blocking their catalytic clefts^{20,21}. PYLs are ABA receptors: in the presence of ABA, PP2C-As form complexes with PYL-ABA, and their activities are thus inhibited²². Such inhibition releases SnRK2s from suppression by PP2C-As, leading to the induced expression of many downstream effectors, such as *RD29B*²³. In the absence of ABA, several PYLs, such as PYL5, PYL6, PYL8, PYL9, and PYL10, can still interact with and inhibit PP2C-As, but the inhibition is weaker than that caused by ABA-bound PYLs²⁴.

In addition to PYLs, Enhancer of ABA Co-receptor 1 (EAR1) and the ROP GTPases ROP11 can enhance the activities of a subset of PP2C-As^{25–27}. Direct suppressors of PP2C-A phosphatase activity have also been identified. The RNA helicase RH8 and the haem-binding protein DOG1 physically associate with and suppress the activity of AHG3 and AHG1, respectively^{28,29}. Despite the numerous enzyme activity regulators identified for PP2C-As, these regulators merely function on several specific PP2C-As. Apart from PYLs, it remains unknown whether other broad-spectrum regulators target multiple PP2C-As.

The FORKED-LIKE (FL) protein family is characterised by an N-terminal auxin canalisation (AC) domain and a C-terminal pleckstrin homology-like (PH) domain^{30,31}. These proteins were initially discovered to be involved in leaf vein development by mediating asymmetric localisation of the auxin efflux protein PINFORMED1 (PIN1)³⁰. Recent studies have highlighted additional functions of FL proteins in plant biology. FL1 and FL3 are interaction partners of the blue light receptor cryptochrome (CRY2). CRY2 physically interacts with FL1 and FL3 to inhibit their ability to promote root elongation³². Our group found that *FL7* transcripts are present across multiple plant tissues, including leaves, roots, stems, flowers, and siliques, with the protein localising in both nuclear and cytoplasmic compartments³³. Furthermore, we found that *FL7* directly interacts with HAI1/2/3 and inhibits their phosphatase activity to prevent the dephosphorylation of MPK3/6, thereby promoting plant immunity³³. This discovery prompted us to investigate whether *FL7*, similar to PYLs, functions as a general enzyme inhibitor of PP2C-As.

In this study, we provide evidence that *FL7* functions as a broad-spectrum inhibitor of PP2C-As in *Arabidopsis* and is thus a positive regulator of the plant ABA response and osmotic tolerance. Importantly, salt stress often impairs plant resistance to pathogens, but we found that *FL7*-overexpressing lines presented increased resistance to salt stress. In contrast to PYLs, *FL7* inhibits PP2C-A activity in an ABA-independent and noncompetitive manner. Consistent with these findings, *FL7* positively regulates the osmotic response independent of ABA. *FL7* potently suppresses PP2C-A phosphatase activity by directly

binding to its C-terminal phosphatase domain via its conserved N-terminal AC domain. Evolutionary analyses revealed that *FL7* homologues emerged in Klebsormidiophyceae green algae and expanded across streptophyte lineages. The algal *FL7* homologues, KnFL7 from *Klebsormidium nitens* and CbFL7 from *Chara braunii*, had PP2C-A inhibitory activity and exhibited functions that were similar to those of AtFL7. These results indicated that *FL7* represents an ancient family of PP2C-A inhibitors that are conserved throughout green plants, predating PYLs, and might integrate plant biotic and abiotic stress responses.

Results

FL7 broadly interacts with PP2C-As and inhibits their phosphatase activity

We previously found that *FL7* is an inhibitor of HAI1/2/3³³, prompting us to test the effect of *FL7* on other PP2C-A members. First, we found that *FL7* could interact with all of the other six PP2C-As in both yeast two-hybrid and coimmunoprecipitation assays, using HAI1s as positive controls and a clade D PP2C (At5g02760) as a negative control (Fig. 1a,b). To confirm the natural interaction between *FL7* and PP2C-As *in planta*, we immunoprecipitated the *FL7* proteins from *pFL7::gFL7-FLAG* *fl7* complementation lines (hereafter *gFL7*). ABI1 and ABI2 proteins could be detected in the precipitates using α -ABI1/ABI2 antibodies (Fig. 1c). Furthermore, we conducted pull-down assays to detect the direct interaction between *FL7* and PP2C-As. We successfully purified the ABI1, ABI2, HAB2, and AHG3 proteins. Unlike the clade D PP2C control, all the purified PP2C-As displayed an affinity for *FL7* in the pull-down assays (Fig. 1d). These results demonstrate that *FL7* is associated with PP2C-As both *in vivo* and *in vitro*. Notably, PYL10 is a broad interactor of PP2C-As²⁴ and was also used as a positive control in the Y2H assay. We found that PYL10 interacts with all the PP2C-As except AHG1, whereas *FL7* can interact with all of them (Fig. 1a).

We then tested whether *FL7* can inhibit the activity of PP2C-As other than HAI1s. The results revealed that *FL7* inhibited between 23 and 56% of the activity of ABI1, ABI2, HAB2, and AHG3 but not that of the clade D enzyme (Fig. 1e), indicating that *FL7* broadly inhibits PP2C-A activity. Given that the N-terminus of some PP2C-As, including ABI1 and AHG3, encompasses an autoinhibitory domain²⁵, we examined whether this region is required for *FL7*-mediated suppression. N-terminal truncated ABI1 (131–434) and AHG3 (106–398) mutants were generated, and their phosphatase activities were higher than those of the wild-type PP2C-As, indicating successful removal of the autoinhibitory domain (Supplementary Fig. 1a). *FL7* still inhibited both the PP2C-A N-terminal truncation mutants (Supplementary Fig. 1a), demonstrating that *FL7* directly suppresses PP2C-A activity independent of its autoinhibitory domain.

We then measured PP2C phosphatase activity among the wild-type, *fl7* and *OE-FL7* lines³³ *in vivo* (Fig. 1f). Our results demonstrated that compared with the wild-type plants, the *FL7* overexpression lines presented significantly reduced PP2C activity, whereas the *fl7* mutant presented the highest activity level (Fig. 1f). Collectively, these biochemical data confirm that *FL7* acts as a broad-spectrum enzyme inhibitor of PP2C-As both *in vivo* and *in vitro*.

FL7 suppresses the dephosphorylation of MPK6 and SnRK2.6 mediated by PP2C-As

We further tested whether *FL7* could suppress the PP2C-A-mediated dephosphorylation of its substrates. Phosphorylated MPK6 can be dephosphorylated by ABI1 (Supplementary Fig. 1b), which is consistent with a previous report¹⁷. In the presence of *FL7*, but not the GST control, MPK6 dephosphorylation by ABI1 was significantly restored (Fig. 1g). As a control, *FL7* alone did not affect MPK6 phosphorylation (Supplementary Fig. 1c).

SnRK2s are well-known substrates of PP2C-As¹³. The phosphorylation level of SnRK2.6 greatly decreased in the presence of ABI1

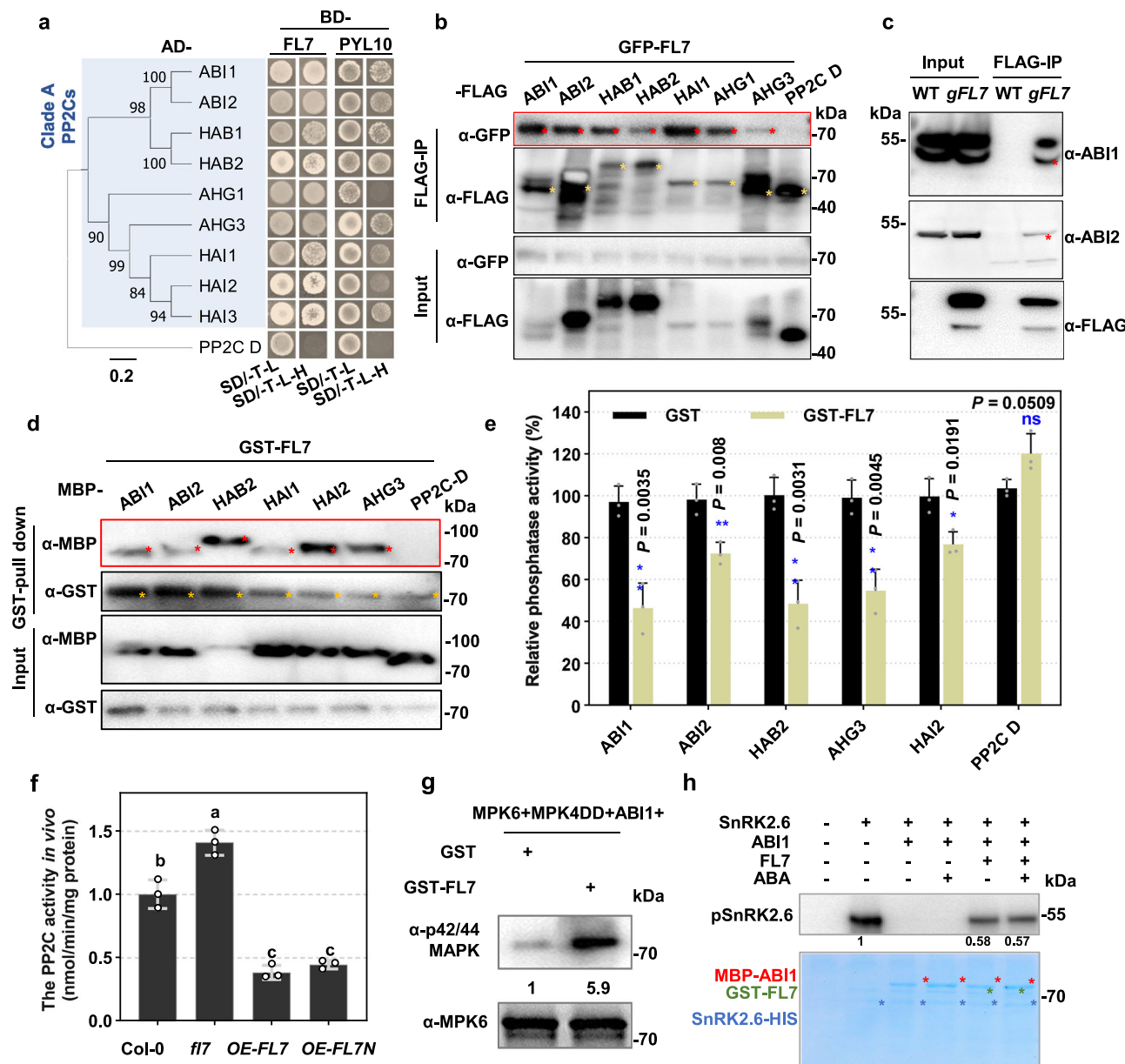


Fig. 1 | FL7 is a general enzyme inhibitor of PP2C-As. **a** Y2H assay. BD-PYL10 was used as positive control. BD-PP2C D (At5g02760) was used as a negative control. **b** Co-IP assay. **c** Natural interaction between ABI1 or ABI2 with FL7 in Arabidopsis seedlings. Total proteins from Col-0 and the gFL7 transgenic plants were immunoprecipitated with anti-FLAG affinity beads. Then the immunoprecipitated proteins were detected with anti-FLAG, ABI1 or ABI2 antibodies. **d** Verification of the interaction between FL7 and PP2C-As by pull-down assay. Interacting protein complexes were immunoprecipitated with anti-GST beads, and the bound proteins were detected by immunoblotting. **e** Inhibition of FL7 on the phosphatase activity of PP2C-As in vitro. Recombinant PP2Cs (2 µg) and FL7 (4 µg) proteins were used for phosphatase activity assays. GST (4 µg) was used as a control. Substrate concentration was 100 µM. Data are means ± SD of three technical replicates ($n=3$; * $P<0.05$, ** $P<0.01$, Student's t test, two-sided, ns not significant). **f** Total PP2C activity in the indicated lines. Total proteins were extracted from 10-day-old

seedlings. PP2C activity is represented as the amount of phosphate dephosphorylated by PP2C released per minute. Data are means ± SD of three biological replicates ($n=3$; lowercase letters indicate significant differences between multiple groups by one-way ANOVA at $P<0.05$ with Tukey's test, the same applies to the subsequent figures). **g** Inhibition of FL7 on ABII-mediated dephosphorylation of MPK6 in vitro. Recombinant MPK6 was phosphorylated by GST-MKK4DD. Phosphorylated MPK6 (500 ng) and MBP-ABII (2 µg) were mixed with GST (4 µg) or GST-FL7 (4 µg) and incubated at 30 °C for 15 min. Proteins were detected by immunoblotting using the indicated antibodies. **h** Inhibition of FL7 on ABII-mediated dephosphorylation of SnRK2.6 in vitro. Phosphorylated SnRK2.6-HIS (1 µg), MBP-ABII (0.5 µg) and/or GST-FL7 (2 µg) were mixed and incubated at 30 °C for 15 min. ABA concentration was 10 µM. Experiments were performed two times with similar results. The experiments in (e-g) were performed two times with similar results. Source data are provided as a Source Data file.

(Fig. 1h, Supplementary Fig. 1d). However, this phenomenon was reversed by the addition of FL7 (Fig. 1h, Supplementary Fig. 1d), indicating that FL7 inhibited SnRK2.6 dephosphorylation by ABII in vitro. To test whether FL7 inhibits the PP2C-A-mediated dephosphorylation of SnRK2.6 in vivo, we conducted dual-luciferase reporter assays in snrk2.2/3/6 triple-mutant protoplasts (Supplementary Fig. 1e) because

phosphorylated SnRK2.6 activates ABF2, which in turn induces RD29B expression²³. The results revealed that the expression of SnRK2.6 increased the pRD29B-LUC output, whereas the addition of ABII and AHG3 suppressed the chemiluminescence signal (Supplementary Fig. 1f). PYL10 was used as a positive control in this assay, and the

addition of PYL10 restored the signals inhibited by ABI1 and AHG3 (Supplementary Fig. 1f).

FL7 positively regulates the plant osmotic stress response

To investigate the function of FL7 as an inhibitor of PP2C-As, we tested the ABA sensitivity of FL7-related genotypes on the basis of the antagonistic effect between total PP2C-A activity and the ABA response²⁵. In the absence of ABA, compared with the wild-type plants, the *f7* mutants and *FL7* overexpression lines (hereafter *OE-FL7*) presented no obvious differences in terms of the germination rate or primary root length (Fig. 2a, Supplementary Fig. 2a). However, compared with the wild-type plants, the ABA treatment increased the *f7* mutant germination rate and primary root growth, whereas the *OE-FL7* seedlings displayed ABA hypersensitivity (Fig. 2a, Supplementary Fig. 2a). Similarly, ABA-induced stomatal closure was impaired in the *f7* mutants but enhanced in the *OE-FL7* lines (Fig. 2b). These results indicated that FL7 positively regulates plant ABA responses, probably through inhibition of total PP2C-A activity.

PP2C-As are vital negative regulators of the plant osmotic response³⁴. We thus explored the role of FL7 in plant osmotic tolerance. Under normal conditions, all the *Arabidopsis* lines exhibited similar growth. After 20 days of drought, the *f7* mutant displayed the lowest survival rate, whereas the *OE-FL7* lines showed significantly increased survival (Fig. 2c), demonstrating that FL7 positively regulates drought tolerance. Similarly, water loss from detached leaves was also more rapid in the *f7* mutant and weakened in the *OE-FL7* lines (Supplementary Fig. 2b). To obtain a genome-wide view of gene expression changes in the *f7* mutant and *OE-FL7* lines in response to osmotic stress, we conducted RNA sequencing (RNA-seq) analysis on Col-0, *f7* and *OE-FL7* lines treated with 300 mM mannitol. After 12 h of treatment, 2035, 2823 and 3314 differentially expressed genes (DEGs) ($|\log_2(\text{fold change})| \geq 1, P < 0.05$) were detected in Col-0, *f7* and *OE-FL7* seedlings, respectively (Supplementary Data 1). The overlapping pattern of DEGs between Col-0, *f7*, and *OE-FL7* seedlings suggested a common osmotic response mechanism among these lines (Fig. 2d). The k-means clustering of all DEGs between Col-0, *f7*, and *OE-FL7* seedlings resulted in six clusters with distinct expression patterns (Supplementary Fig. 3). Cluster 3 included genes whose expression was strongly induced by mannitol in the *OE-FL7* line but weakly induced in both the Col-0 and *f7* lines. The genes in Cluster 6 exhibited the strongest mannitol-induced expression in the *OE-FL7* line, moderate induction in Col-0, and the weakest induction in the *f7* mutant (Supplementary Fig. 3). Gene Ontology (GO) enrichment analysis of the DEGs in Clusters 3 and 6 revealed that these genes were highly enriched in potential abiotic stress response-related GO terms such as “response to abiotic stimulus” and “response to stress” (Supplementary Fig. 3). Moreover, these clusters are enriched in many plant osmotic response marker genes, such as *ABI1/2*, *RD29B* and *RAB18*³⁵ (Supplementary Fig. 3). These marker genes generally exhibited the strongest mannitol-induced expression in the *OE-FL7* line, moderate induction in Col-0, and the weakest induction in the *f7* mutant (Fig. 2e). These results indicated that FL7 positively regulates the plant osmotic response.

Enhanced pathogenic resistance of FL7-overexpressing lines is not impaired by salt stress

We previously reported that FL7 is a positive regulator of plant immunity³³. Combined with the data presented here, these findings reveal that FL7 is a positive hub regulator of both the osmotic response and the defence response, indicating that FL7 might be a promising genetic resource for the development of resistant plants suitable for saline soils. We first tested the role of FL7 in plant salt tolerance and found that FL7 promotes plant tolerance to salinity stress caused by NaCl through assays of electrolyte leakage (Fig. 2f). Activation of SnRK2s is a central step in the plant response to salt stress, and we

found that NaCl-induced SnRK2.2, SnRK2.3, and SnRK2.6 phosphorylation was reduced in the *f7* mutant but increased in the *OE-FL7* lines (Supplementary Fig. 4a). To test whether FL7 responded to salt stress, we analysed its protein accumulation level in *OE-FL7* and *gF7* plants after NaCl treatment. The FL7 protein level increased with treatment (Supplementary Fig. 4b). These results indicated that FL7 responses to and positively regulates plant salt tolerance.

We next tested whether FL7 could promote plant immunity under salt stress. Four-week-old *Arabidopsis* plants were irrigated with water that contained 100 mM NaCl to simulate soil salinization, and the leaves were detached for the inoculation assay at 24 h post-treatment (Supplementary Fig. 4c). In the absence of NaCl treatment, the *f7* mutant was more susceptible, whereas the *OE-FL7* line was more resistant to *Phytophthora capsici* (Fig. 2g), supporting FL7 as a positive plant immune regulator. After NaCl treatment, the susceptibility of the wild-type, *f7* mutant and *gF7* complementation lines to *P. capsici* significantly increased (Fig. 2g), which is consistent with previous findings that soil salinization increased disease severity caused by *Phytophthora parasitica* and *P. cryptogea*⁴. Interestingly, no obvious lesion area changes could be detected in the *OE-FL7* lines after mock or NaCl treatment, indicating that the degree of immune weakness caused by NaCl treatment greatly decreased in the *OE-FL7* plants (Fig. 2g).

Genetic analysis of *f7* with the *pp2c-As* mutants

To further analyse the genetic relationship between FL7 and PP2C-As, we knocked out FL7 in the *abi1 hab1 pp2ca* triple mutant using CRISPR-Cas9, generating an *abi1 hab1 pp2ca f7* quadruple mutant (Supplementary Fig. 4d). The *abi1 hab1 pp2ca* triple mutant is sensitive to ABA during seed germination and root growth (Fig. 3a, b), which is consistent with previous reports¹⁵. Although *f7* showed reduced ABA sensitivity compared with wild-type, the *abi1 hab1 pp2ca f7* quadruple mutant exhibited a phenotype comparable to that of the *abi1 hab1 pp2ca* triple mutant (Fig. 3a, b). Similarly, a drought tolerance analysis revealed that the *abi1 hab1 pp2ca f7* quadruple mutant displayed a phenotype comparable to that of the *abi1 hab1 pp2ca* triple mutant, with both showing enhanced drought tolerance (Fig. 3c). These results indicate that FL7 functioning is dependent mainly on PP2C-As.

FL7 inhibits PP2C-As in an ABA-independent and noncompetitive manner

ABA promotes the inhibition of PP2C-As by PYLs²². However, our phosphatase activity indicated that the inhibitory function of FL7 is independent of ABA (Fig. 1e) – in contrast to that of canonical PYLs. To further test whether ABA is required for FL7 function, a microscale thermophoresis binding assay was conducted by using PYL10 as a positive control. The results revealed an interaction between ABA and PYL10 but no binding affinity for ABA for the FL7 and GST control (Fig. 4a). We then tested whether ABA influences the interaction between FL7 and PP2C-As. Consistent with previous findings²², ABA stimulated PYL10-ABI1 complex formation (Fig. 4b). In contrast, ABA did not affect FL7-ABI1 associations (Fig. 4b). We next investigated whether ABA regulates FL7 inhibition of PP2C-A activity. Enzymatic analyses demonstrated that ABA bolstered PYL10-mediated but not FL7-mediated inhibition of ABI1 (Fig. 4c). Similar ABA-independent inhibition activity was observed for FL7 when ABI2 and AHG3 were used (Supplementary Fig. 5a, b). Furthermore, ABA did not enhance the ability of FL7 to suppress ABI1-mediated dephosphorylation of SnRK2.6 (Fig. 1h, Supplementary Fig. 1d). These results indicated that the inhibitory activity of FL7 on PP2C-As is independent of ABA.

To elucidate the biochemical mechanisms underlying the inhibitory activities of FL7 and PYL10, we performed enzyme kinetic analyses (Fig. 4d). Competitive inhibitors compete with substrate(s) for the active site of the enzyme, and the inhibition is reversible upon substrate saturation. In contrast, noncompetitive inhibitors alter active

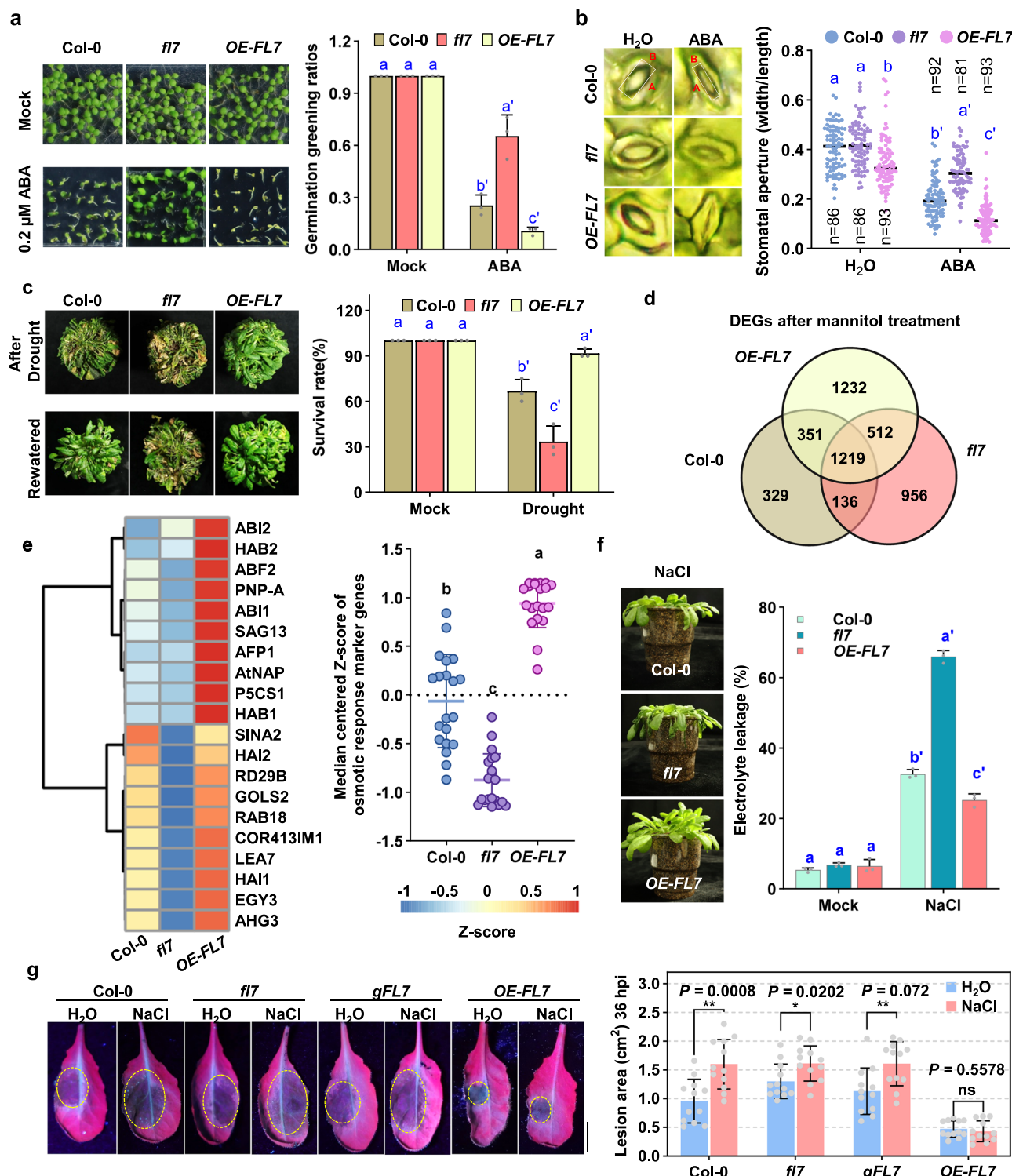


Fig. 2 | FL7 positively regulates plant osmotic stress response. **a** Germination phenotypes. Data are means \pm SD of three biological replicates, with each replicate containing at least 30 seedlings (two-way ANOVA with Tukey's test; $P < 0.05$).

b Stomatal aperture of plant treated with ABA. Epidermal strips with fully open stomata were treated with or without 20 μ M ABA for 2 h before being photographed (left). Stomatal aperture (the ratio of width B to length A marked in red in figure) was quantified from each genotype (right). Data are means \pm SD (two-way ANOVA with Tukey's test; $P < 0.05$). Experiments were performed three times with similar results. **c** Drought phenotypes of Col-0, f17 and OE-FL7 lines in soil. Data represent means \pm SD from three biological replicates, with each replicate containing at least 20 plants (two-way ANOVA with Tukey's test; $P < 0.05$). **d** Overlaps of DEGs from indicated lines treated with mannitol. The numbers accounted for genes

shared by different subsets. **e** Heat map of mean-centred Z-scores for osmotic response marker genes arranged following k-means clustering. Box plot indicates the relative expression level based on median centred Z-score of osmotic response marker genes (right) (Data are means \pm SD, $n = 20$, one-way ANOVA with Tukey's test; $P < 0.05$). **f** Electrolyte leakage rate of plants treated with NaCl. Four-week-old plants were irrigated with saline water for a week. Data are means \pm SD of three technical replicates (two-way ANOVA with Tukey's test; $P < 0.05$). Experiments were performed three times with similar results. **g** The *P. capsici* inoculation phenotypes. Data are means \pm SD ($n = 12$ leaves per group; * $P < 0.05$, ** $P < 0.01$, Student's *t* test, two-sided, ns not significant). The experiments were performed two times with similar results. Scale bar = 1 cm. Source data are provided as a Source Data file.

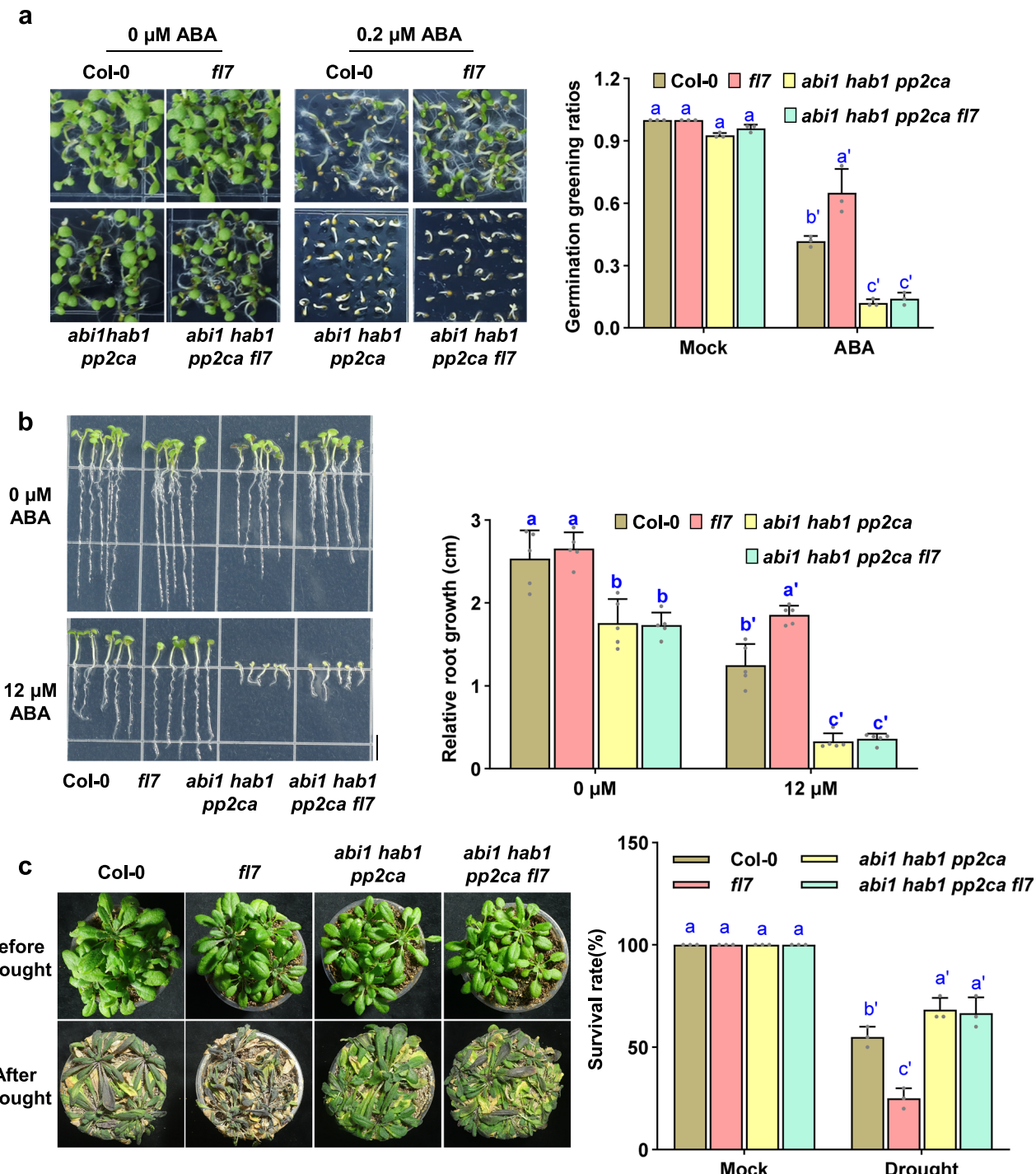
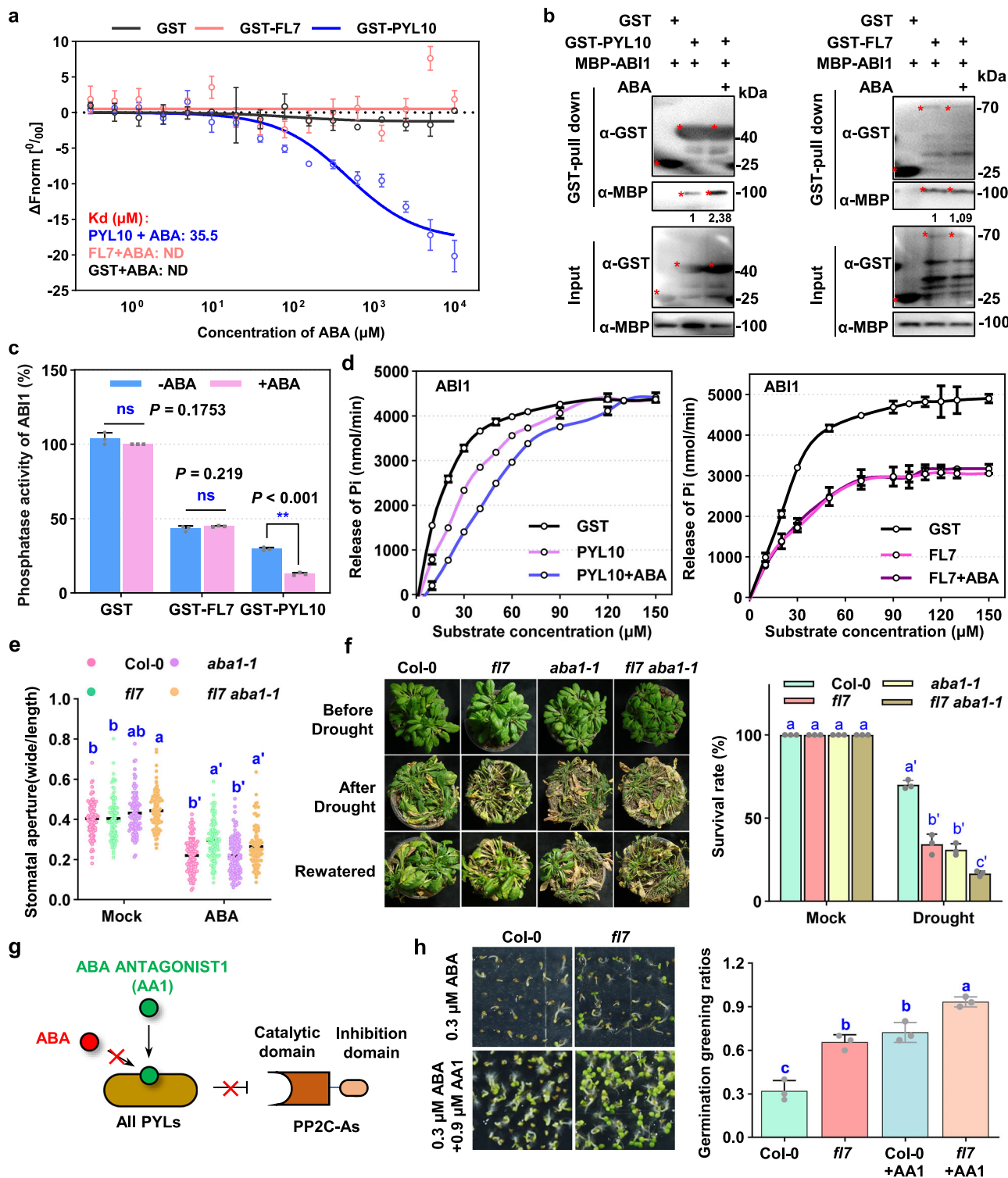


Fig. 3 | Genetic analysis of fl7 with the pp2c-As mutants. a Germination phenotypes of *abi1 hab1 pp2ca* and *abi1 hab1 pp2ca fl7* lines. The seeds were germinated on 1/2 MS medium with or without ABA for 7 days. Data are means \pm SD of three biological replicates, with each replicate containing at least 30 seedlings (two-way ANOVA with Tukey's test, $P < 0.05$). **b** Root growth phenotypes of Col-0, *fl7*, *abi1 hab1 pp2ca* and *abi1 hab1 pp2ca fl7* lines treated with ABA. Seeds were germinated on 1/2 MS medium and then transferred to 1/2 MS medium containing 12 μ M ABA and vertically grown for additional 5 days. The length of root was measured with Image J. Data are mean \pm SD ($n = 5$; two-way ANOVA with Tukey's test, $P < 0.05$). Scale bar = 0.5 cm. The experiments were performed three times with similar results. **c** Drought tolerance of Col-0, *fl7*, *abi1 hab1 pp2ca* and *abi1 hab1 pp2ca fl7* lines. Data represent means \pm SD from three biological replicates, with each replicate containing at least 20 plants (two-way ANOVA with Tukey's test, $P < 0.05$). Source data are provided as a Source Data file.

and vertically grown for additional 5 days. The length of root was measured with Image J. Data are mean \pm SD ($n = 5$; two-way ANOVA with Tukey's test, $P < 0.05$). Scale bar = 0.5 cm. The experiments were performed three times with similar results. **c** Drought tolerance of Col-0, *fl7*, *abi1 hab1 pp2ca* and *abi1 hab1 pp2ca fl7* lines. Data represent means \pm SD from three biological replicates, with each replicate containing at least 20 plants (two-way ANOVA with Tukey's test, $P < 0.05$). Source data are provided as a Source Data file.

site conformation or chemistry to reduce substrate binding/catalysis independently of substrate levels (Supplementary Fig. 5c)³⁶. Consistently, ABA did not increase FL7 inhibition in this assay (Fig. 4d). In contrast to the reversible inhibition of ABI1 by PYL10 upon substrate saturation despite the presence of ABA, FL7-mediated ABI1

suppression was unresponsive to both increased substrate availability and increased ABA treatment (Fig. 4d). Identical patterns also occurred for AHG3 (Supplementary Fig. 5d), corroborating a noncompetitive inhibition mechanism for FL7.



FL7 enhances plant osmotic stress tolerance through an ABA-independent pathway

To investigate whether FL7 regulates the plant osmotic response independently of ABA, we crossed the ABA-deficient *aba1-1* mutant with *f17* to generate the *f17 aba1-1* double mutant (Supplementary Fig. 5e, f). We found that, in the absence of ABA, the stomata of *aba1-1* were more open than those of *f17* and Col-0 were, while the stomatal aperture of the *f17 aba1-1* double mutant was the largest (Fig. 4e). Drought tolerance assay revealed that compared with the *aba1-1* single mutant, the *f17 aba1-1* double mutant had lower survival rates (Fig. 4f, Supplementary Fig. 5g). These results further support that

FL7 suppresses PP2C-A activity and positively regulates the plant osmotic response in an ABA-independent manner.

PYLs function as ABA receptors and broad suppressors of PP2C-As²². To examine the relationship between FL7 and PYLs, we employed ABA ANTAGONIST1 (AA1), a broad-spectrum antagonist that blocks all PYR/PYL-PP2C interactions³⁷ (Fig. 4g). We analysed the germination rates of Col-0 and *f17* mutant seeds grown on 1/2 MS plates supplemented with either ABA alone or ABA plus AA1. The addition of AA1 significantly increased the germination rate of Col-0, indicating successful inhibition of PYL activity (Fig. 4h). Notably, the germination rate of *f17* + AA1 was higher than that of Col-0 + AA1 (Fig. 4h),

Fig. 4 | FL7 inhibits PP2C-As through an ABA-independent noncompetitive mechanism. **a** Binding affinity of ABA with FL7 or PYL10 in MST assay. The data points indicate the fraction of ABA-bound proteins at different ligand concentrations, and the curves indicate the calculated fits (Data are means \pm SD, $n = 3$). The mean values of the equilibrium dissociation constant (K_d) are shown in the panel. **b** Effect of ABA on the interaction between ABI1 with PYL10 or FL7 in pull-down assay. ABA concentration was 10 μ M. Numbers below the blots represent the blot band intensity. **c** Inhibition of FL7 or PYL10 on ABI1 with or without ABA. Recombinant ABI1 (2 μ g) and FL7 or PYL10 (4 μ g) proteins were used. Substrate concentration was 100 μ M and ABA concentration was 10 μ M. Data are means \pm SD of three technical replicates ($n = 3$; ** $P < 0.01$, Student's t test, two-sided, ns not significant). **d** Kinetic of ABI1 phosphatase activity. Recombinant proteins of ABI1 (2 μ g) and FL7 (4 μ g) were used for phosphatase activity assays. ABA concentration

was 10 μ M. Data are means \pm SD of three technical replicates. **e** Stomatal aperture of plant treated with or without ABA. Data are mean \pm SD of three independent experiments ($n = 100$, two-way ANOVA with Tukey's test; $P < 0.05$). **f** The plant phenotype in responses to drought stress. Data are mean \pm SD of three biological replicates ($n = 3$; two-way ANOVA with Tukey's test; $P < 0.05$). **g** The working model of AA1. AA1 binding to PYLs to block their inhibition activity on PP2C-As. **h** Germination phenotypes of the indicated lines in response to ABA with or without AA1. Seeds were grown on 1/2 MS medium supplemented with ABA alone (0.3 μ M) or in combination with AA1 (0.9 μ M) for 7 days. Data are means \pm SD of three biological replicates, with each replicate containing at least 30 seedlings (one-way ANOVA with Tukey's test; $P < 0.05$). All experiments were performed three times with similar results. Source data are provided as a Source Data file.

suggesting that FL7 continues to regulate the PP2C pathway even when PYL activity is blocked. In addition, we found that the presence of both PYL and FL7 led to a stronger inhibition of ABI1 phosphatase activity compared with either component alone, indicating an additive effect (Supplementary Fig. 5h). Collectively, these data support that FL7 and PYLs function in parallel pathways.

FL7 inhibits PP2C activity through an N-terminal auxin canalisation domain

The FL7 protein contained an N-terminal auxin canalisation domain (AC) and a C-terminal pleckstrin homology-like domain (PH) (Fig. 5a). To investigate which domain of FL7 is critical for the inhibitory activity on PP2C-As, we generated FL7 truncation mutants (FL7N and FL7C) (Fig. 5a). ABI1 and AHG3 were selected as representatives of PP2C-As to test their interactions with FL7 truncation mutants. The results showed that the AC domain, but not the PH domain, sufficiently interacted with the phosphatase domain of the tested PP2C-As in a Y2H assay (ABI1N for the autoinhibition domain; ABI1C for the phosphatase domain) (Fig. 5a, Supplementary Fig. 6a). Similarly, the AC domain was sufficient to suppress the activities of ABI1 and AHG3 (Fig. 5b, Supplementary Fig. 6b), and this inhibitory activity was not enhanced by ABA (Fig. 5c, Supplementary Fig. 6c). Furthermore, we added the AC domain or the PH domain of FL7 under the control of the native promoter of *FL7* to the *f7* mutant line (Supplementary Fig. 6d). The AC domain, but not the PH domain, completely restored the *f7* mutant phenotype, while overexpression of the AC domain mimicked the phenotype of the *OE-FL7* lines (Fig. 5d–f, Supplementary Fig. 6e–g). Compared with the *OE-FL7* lines, the protein extracts of *OE-FL7N* lines also exhibited impaired PP2C activity (Fig. 1f). These results indicated that the AC domain is sufficient for the suppression of PP2C activity.

FL7 emerged in an ancient streptophyte

When did FL7 evolve? To investigate the conservation of FL7, we performed comparative genomic and phylogenetic analyses of the AC domain in the genomes of 17 representative plant species that cover a broad diversity of plants (Fig. 6a; Supplementary Data 2). Using a Markov model of the AC domain generated by the Pfam database, we identified a total of 32 FL7 homologues with the AC domain in the genomes of 9 plants (Fig. 6a; Supplementary Data 3 and 4). The number of FL7 homologues we identified in *Arabidopsis* aligns with previous reports³⁰, bolstering the identification stability of our approach. In addition to the land plant clade, homologues of FL7 were found in the streptophyte algal families Klebsormidiophyceae and Charophyceae but not in the phragmoplastophytic Coleochaetophyceae and Zygnematophyceae or the clade of Mesostigmatophyceae and Chlorokybophyceae (Fig. 6a). We performed a large-scale phylogenetic analysis of these proteins with the AC domain. We found that plants formed a monophyletic group with high support values (Fig. 6a). The copy number of FL7 homologues is low in algal and bryophyte species but is expanded in vascular plants (Fig. 6a, b), indicating that FL7 homologues are monophyletic.

PYLs originated in the common ancestor of Zygnematophyceae and land plants³⁸ and were likely gained by horizontal gene transfer from soil bacteria³⁹. Interestingly, FL7 homologues were identified in Klebsormidiophyceae, suggesting that they emerged in a last common ancestor (LCA) of Klebsormidiophyceae and Phragmoplastophyta, which likely lived more than a billion years ago⁴⁰. These findings indicate that FL7 homologues might be more ancient PP2C inhibitors than PYLs are. To further study FL7 homologues in streptophyte algae, we performed similarity searches and phylogenetic analyses within six charophyte transcriptomes^{41,42}. We found that FL7 homologues are present in representatives of two other charophyte genera: *Nitella*, another Charophyceae, and, importantly, *Coleochaete*, a Coleochaetophyceae (Supplementary Data 5). These findings further underscore the emergence of FL7 homologues in the LCAs of Klebsormidiophyceae and Phragmoplastophyta. Since the absence of one gene in the transcriptome of one species does not guarantee its absence in that species⁴³, it might be that FL7 homologues are even more widespread in streptophytes. Our results further demonstrate that the AC domain is widely present in streptophyte algae. Although some plant FL7 homologues lack a PH domain (Fig. 6a; Supplementary Data 4), these proteins cluster with those with PH domains in the phylogenetic tree (Fig. 6a), indicating that they might have arisen from AC-PH proteins by deleting PH. Taken together, our comparative genomic analyses provide evidence for the deep evolutionary origin of FL7 homologues in a streptophyte predating PYLs (Fig. 6b).

FL7 function is conserved across a billion years of streptophyte evolution

PYL was an evolutionary innovation of a common ancestor of Zygnematophyceae and land plants^{39,44}. Interestingly, our evolutionary analysis revealed that compared with PYLs, FL7 homologues are more ancient PP2C inhibitors. To investigate their conserved function across streptophytes, we synthesised FL7s from the two streptophyte algae *Klebsormidium nitens* and *Chara braunii*. Y2H and pull-down assays revealed that, like AtFL7, algal FL7s also interact with AtABI1 (Fig. 7a, b). Furthermore, algal FL7 inhibited the activity of AtABI1 (Fig. 7c), indicating that the function of algal FL7 is conserved with AtFL7. We constructed transgenic plants in which the algal FL7s were under the control of the AtFL7 promoter and introduced them into the *f7* mutant (Supplementary Fig. 7a, b). Compared with the wild-type plants, the complemental lines presented a similar osmotic response (Fig. 7d, e). Thus, our results indicated that FL7 is a functionally conserved PP2C-A inhibitor across a billion years of streptophyte evolution.

Discussion

To survive in unfavourable environments, plants activate diverse adaptive processes to prevent osmotic stress and pathogen colonization, among which PP2C-As are key modulators⁴⁵. Here, we report that a broad-spectrum PP2C-A interactor, FL7, functions as a direct inhibitor of PP2C-A activity through its N-terminal AC domain. Interestingly, the function of FL7 inhibition differs from that of PYLs in two

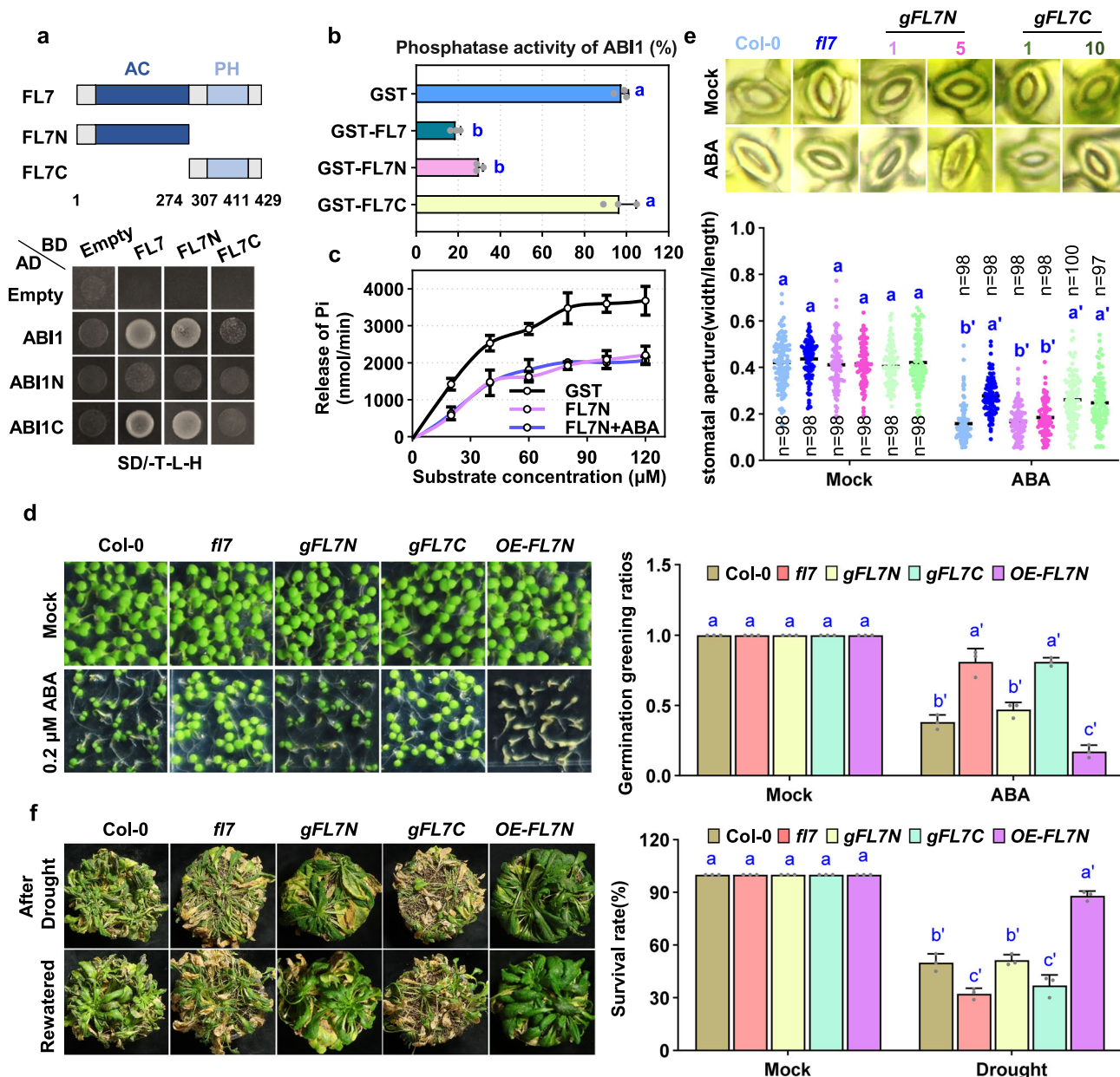


Fig. 5 | FL7 inhibits PP2Cs activity through an N terminal auxin canalisation domain. **a** Verification of the interaction between FL7 and ABI1 by Y2H. Schematic diagram of ABII, FL7 proteins, and related truncations is shown in the upper panel. **b** Inhibition of phosphatase activity of ABI1 by FL7 protein and related truncations. Recombinant ABI1 (2 μg) and FL7 or related truncation proteins (4 μg) were used for phosphatase activity assays. GST (4 μg) was used as a control. Substrate concentration was 100 μM. Data are means ± SD of three technical replicates (one-way ANOVA with Tukey's test; $P < 0.05$). Experiments were performed three times with similar results. **c** Kinetic of ABI1 phosphatase activity in the presence of FL7N. The calculated K_m of ABI1, ABI1 + FL7N, ABI1 + FL7N + ABA was 47.62 μM, 71.51 μM and 51.77 μM, respectively, and the V_{max} was 5301 nmol/min, 3593 nmol/min and 3123 nmol/min, respectively. Data are means ± SD ($n = 3$). The experiments were

performed three times with similar results. **d** Germination phenotypes of Col-0, fl7, gFL7N, gFL7C and OE-FL7N lines. The seeds were germinated on 1/2 MS medium without or with ABA for 7 days (left). Data are means ± SD of three biological replicates, with each replicate containing at least 30 seedlings (two-way ANOVA with Tukey's test, $P < 0.05$). **e** ABA-promoted stomatal closure of Col-0, fl7, gFL7N and gFL7C lines. Data are means ± SD (two-way ANOVA with Tukey's test, $P < 0.05$). Experiments were performed three times with similar results. **f** Drought phenotypes of Col-0, fl7, gFL7N, gFL7C and OE-FL7N lines. Data represent means ± SD from three biological replicates, with each replicate containing at least 20 plants (two-way ANOVA with Tukey's test, $P < 0.05$). Source data are provided as a Source Data file.

ways: FL7 inhibition of PP2C-A is independent of ABA and occurs in a noncompetitive manner. Furthermore, FL7 positively regulates osmotic tolerance in an ABA-independent manner. The *FL7*-overexpressing lines were highly resistant to pathogens that could not be impaired by osmotic stress (Fig. 7f). Finally, we found that FL7 is a conserved PP2C inhibitor that emerged more than a billion years ago (Fig. 6b). The functions of FL7 homologues from streptophyte algae are similar to those in *Arabidopsis*.

Soil salinity is an increasingly severe global problem as a result of improper irrigation practices and climate change. The effects of such environmental variables on plants can have negative impacts on plant disease development¹. Identifying key regulators that integrate osmotic stress and defence responses could aid in the development of resistant crops adapted to climate change. Here, we demonstrate that overexpression of FL7, a PP2C-A inhibitor, facilitates plant adaptation to both abiotic and biotic stress. More importantly, *FL7* overexpression

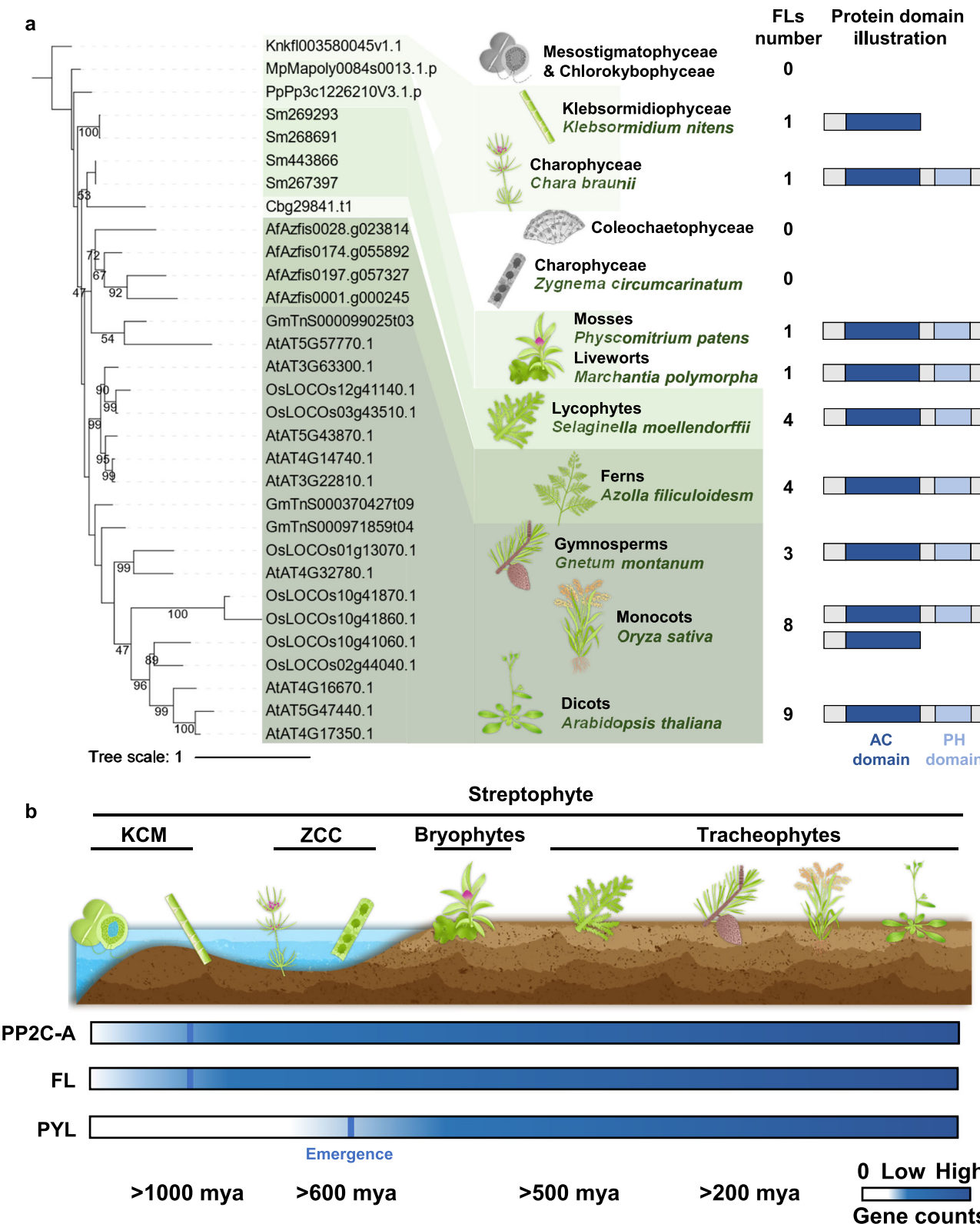


Fig. 6 | FL7 is conserved across streptophyte. **a** Genomic and phylogenetic analyses of FL proteins in representative plant species. The evolutionary tree of FL proteins is shown on the left. The FL gene number identified in indicated species are shown adjacent to the species illustration. The structural analysis of FL proteins in the indicated species are shown on the right. **b** Overview of the evolution of PP2C-A, FL, and PYL genes in plants. White bars indicate the existence of presumed 'ancestral genes' for each gene in algae that cannot be phylogenetically grouped into those of land plants. Blue bars indicate the existence of orthologous genes identified by phylogenetic and/or functional analysis. Emergence of subfamilies is also indicated. Source data are provided as a Source Data file.

PP2C-A, FL, and PYL genes in plants. White bars indicate the existence of presumed 'ancestral genes' for each gene in algae that cannot be phylogenetically grouped into those of land plants. Blue bars indicate the existence of orthologous genes identified by phylogenetic and/or functional analysis. Emergence of subfamilies is also indicated. Source data are provided as a Source Data file.

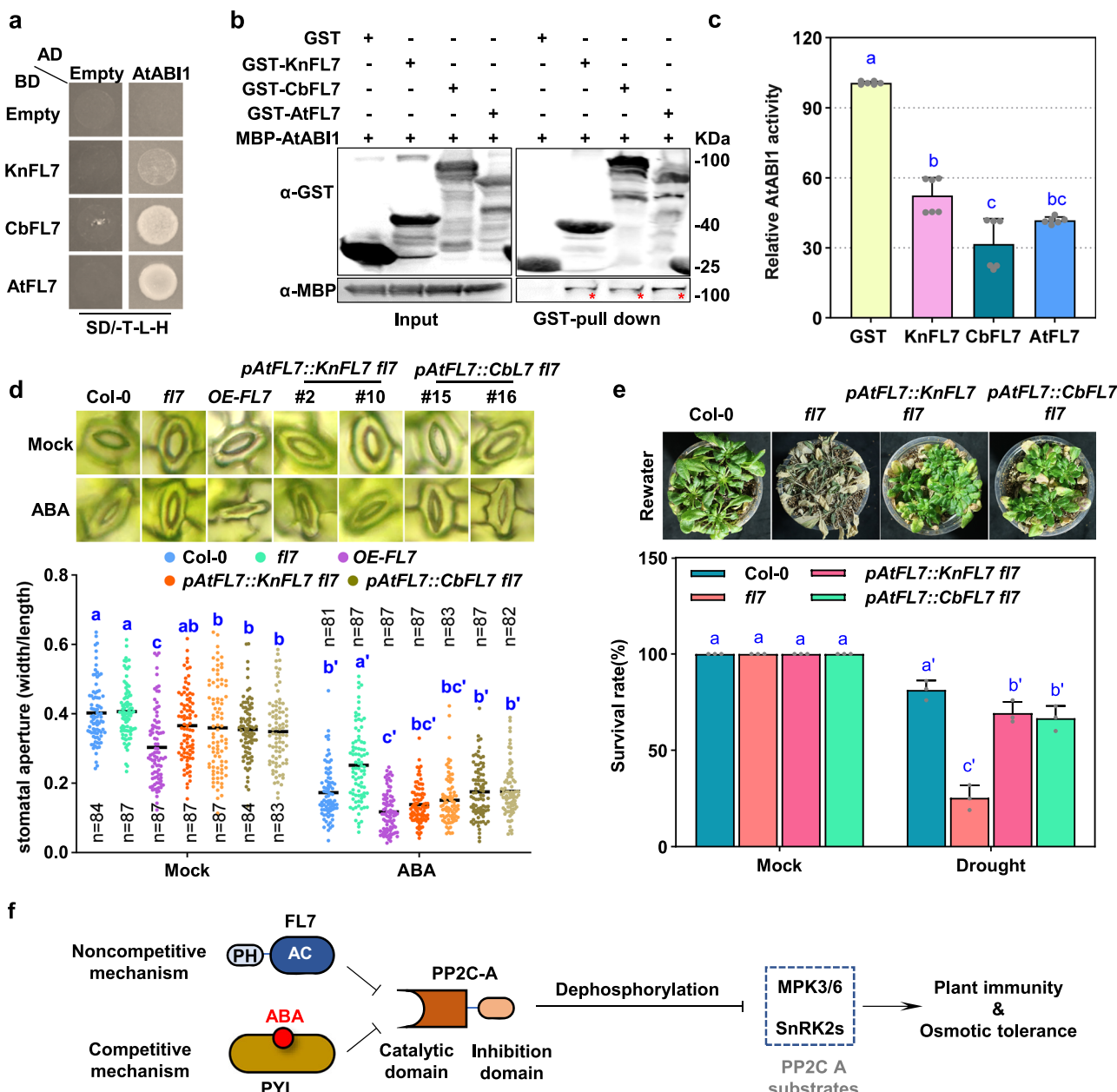


Fig. 7 | FL7s are functionally conserved in Klebsormidiophyceae and Charophyceae. **a, b** Interaction between ABI1 with FL7 homologs from Klebsormidiophyceae and Charophyceae. The interaction between KnFL7 or CbFL7 with AtABI1 were confirmed by Y2H (a) and pull down assay (b). AtFL7 was used as positive control. **c** Algae FL7 inhibits the phosphatase activity of AtABI1 in vitro. Recombinant AtABI1 (2 µg) was mixed with GST (4 µg) or GST-KnFL7/CbFL7/AtFL7 (4 µg) for phosphatase activity assays. The phosphatase activity of AtABI1 without FL7s was set to 100%. Substrate concentration was 100 µM. Data are means \pm SD of six technical replicates ($n = 6$; * $P < 0.05$, ** $P < 0.01$, Student's *t* test, two-sided, ns not significant). The experiments were performed three times with similar results. **d** ABA-promoted stomatal closure of Col-0, *f17*, *pAtFL7::KnFL7 f17* and *pAtFL7::CbFL7 f17* lines. Stomata were observed and photographed using confocal microscope (Top). Data are

means \pm SD (two-way ANOVA with Tukey's test, $P < 0.05$). Experiments were performed three times with similar results. **e** Drought tolerance of Col-0, *f17*, *pAtFL7::KnFL7 f17* and *pAtFL7::CbFL7 f17* lines. Data represent means \pm SD from three biological replicates, with each replicate containing at least 20 plants (two-way ANOVA with Tukey's test, $P < 0.05$). **f** Schematic diagram illustrating FL7 acts as an inhibitor of PP2C-As. FL7 inhibits activity of PP2C-As independent of their auto-inhibition domain. In contrast to canonical PP2C-A inhibitor PYLs, FL7 does not bind to ABA and inhibits PP2C-As in noncompetitive mechanism. When plants are exposed to pathogens or osmotic stress, FL7 accumulates at translation level, inhibiting the phosphatase activity of PP2C-As and enhancing MPK3/6 and SnRK2s activity, ultimately activating immunity to pathogen and resistance to osmotic stress. Source data are provided as a Source Data file.

prevents the impairment of plant immunity by salt stress (Fig. 2g), indicating that FL7 might be a good genetic resource for improving the plant defence response under saline conditions. However, as endogenous FL7 also accumulated under salinity but its resistance was impaired by salinity, we assumed that the high level of FL7 accumulation prior to salinity stress might be critical for conferring resistance to pathogens under salinity. Future research should focus on fine-tuning FL7 protein levels to promote pathogen resistance under

salinity but avoid potential side effects. Such findings highlight the strategy of inhibiting negative hub regulators, such as PP2C-As, in plant responses to biotic and abiotic stresses, which might aid in the development of crops adapted to fluctuating environments caused by climate change.

Interestingly, FL7 inhibited PP2C-As in an ABA-independent manner. In addition to ABA-dependent pathways, ABA-independent pathways are important adaptive mechanisms in plants^{13,46}. For

example, the *ahg1-1* mutant has no ABA-related phenotype in adult plants⁴⁷. Such a function of AHG1 might result from its specific interaction surface with PYLs, leading it to interact only with RCAR1-3¹². Although ABA-bound RCAR1-3 interacts with AHG1, it only weakly inhibits AHG1 activity¹². Unlike PYLs, DOG1 can interact with AHG1 and suppress its activity in parallel with the ABA pathway⁴⁸. Here, we found that FL7 inhibits PP2C-As in an ABA-independent manner and that FL7 also interacts with AHG1 (Fig. 1a), indicating that FL7 interacts with PP2C-As in a different way than PYLs do. This assumption could be further proven by the observation that FL7 inhibits PP2C-As and osmotic tolerance in a noncompetitive manner, which is also different from the activity of PYLs (Fig. 4d). Importantly, mutation of FL7 in the ABA-deficient *aba1-1* mutant further weakened the impaired osmotic tolerance of *aba1-1* (Fig. 4f), indicating that FL7 is involved in the ABA-independent osmotic response.

How plants adapted to living on land is a long-standing question. The evolution of the PP2C-A-regulated pathway is considered a key step in plants' ability to adapt to terrestrial environments⁴⁹. PP2C-As show high functional conservation among all streptophyte species, including algae such as the Klebsormidiophyceae and Charophyceae^{50,51}. However, PYLs originated in the common ancestor of Zygnetophyceae and embryophytes and were obtained by horizontal gene transfer from soil bacteria^{39,44}. This raises the question of how ancient algae such as *K. nitens* and *C. braunii*, which lack a PYL system, regulate PP2C-A activity, causing them to suffer from osmotic stress. Here, we showed that FL7 is a conserved PP2C-A inhibitor throughout Streptophyta and that FL7 homologues from *K. nitens* and *C. braunii* also exhibit PP2C-A inhibition ability (Fig. 7a–e), indicating that FL7 homologues are ancient PP2C-A regulators that might have been used by early algae to regulate PP2C-A activity and adapt to osmotic stress. This assumption could be proven by investigating the biological function of FL7 homologues in these algae in the future. Furthermore, the FL7 homologues expanded during plant terrestrialization (Fig. 6a, b). Notably, treatment of the *fl7* mutant with the general PYL inhibitor AA1 further impaired ABA sensitivity, suggesting that FL7 continues to regulate the PP2C pathway even when PYL activity is blocked (Fig. 4h). These findings indicate that the FL7-PP2C module may represent another important regulatory branch parallel to the ABA-PYL pathway in plant terrestrial adaptation and might help plants regulate ABA-independent PP2C-A regulatory pathways.

The FL family expanded during land plant evolution. In *Arabidopsis*, FL7 is one of nine FKD1/FL proteins. The other FLs also contain an AC domain (Fig. 6a) and thus might also be PP2C-A inhibitors. There might be functional redundancy between FLs. FLs may interact with PP2C-As to form a complex network, thus potentially facilitating responses to a plethora of physiological and developmental processes and environmental stresses. Unravelling this network will require considerable future investigation.

Collectively, our data indicate that FL7 homologues represent an ancient PP2C-A inhibitor family conserved throughout green plants and integrate plant biotic and osmotic responses.

Methods

Plant materials and growth conditions

Arabidopsis plants were grown and maintained in plant growth chambers at an ambient temperature of 23 °C under a 16-h light/8-h dark photoperiod. Light was provided by white fluorescent bulbs with an intensity of ~120 μmol/m²/s. All *Arabidopsis* lines used in this study were from a Col-0 accession. T-DNA insertion mutants were obtained from Arashare (<https://www.arashare.cn/index/>).

We previously obtained *fl7*, *OE-FL7*, *gFL7*, *abi1 hab1 pp2ca* and *snrk2.2/3/6* triple mutants^{33,52,53}. The 1000 bp FL7 promoter (*pFL7*) was amplified from Col-0 genomic DNA. The sequences of *KnFL7* and *CbFL7* were synthesised by a biological company. The coding sequences of FL7 and PYL10 were subsequently cloned via RT-PCR. To

generate complementation transgenic lines expressing FLAG-tagged *pFL7:FL7N*, *pFL7:FL7C*, *pFL7:KnFL7* and *pFL7:CbFL7*, DNA fragments encoding these sequences were fused to a C-terminal 3 × FLAG tag and cloned and inserted into the pCambia1300 vector. To generate transgenic lines overexpressing FLAG-tagged FL7N, the sequence encoding FL7N was fused to a C-terminal 3 × FLAG tag and cloned and inserted into the pCambia1300 vector. All the constructs were subsequently introduced into *Agrobacterium* (*Agrobacterium tumefaciens*) strain GV3101 for plant transformation using the floral dip method. Positive transformants were recovered by antibiotic selection and confirmed by genomic PCR. The *abi1 hab1 pp2ca fl7* quadruple mutant was generated by knocking out *FL7* in the *abi1 hab1 pp2ca* triple mutant using CRISPR-Cas9. To generate the *fl7 aba1-1* double mutant, an *fl7* T-DNA insertion mutant (SALK_07717C) was crossed with an *aba1-1* T-DNA insertion mutant (SALK_027326C). The primers used in this study are listed in Supplementary Data 6.

For the root growth assay, the corresponding seeds were germinated on 1/2 MS medium. After incubation at 4 °C for 3 days, the seeds were transferred to a greenhouse with a 16-h light/8-h dark cycle for an additional 3 days. Seedlings with similar root lengths were then transferred to 1/2 MS medium supplemented with various concentrations of ABA and vertically grown for an additional 5 days. The root lengths were measured using ImageJ software.

For the germination assays, seeds were sown on 1/2 MS medium supplemented with ABA and incubated at 4 °C for 3 days. Unless otherwise stated, a concentration of 0.2 μM ABA was used for all germination assays. The plates were then transferred to a greenhouse and grown for an additional 7 days before determining the seed germination ratio. For the experiment shown in Fig. 4h, a concentration of 0.3 μM ABA was employed, as this assay was conducted following the relocation of our laboratory, during which it was determined that 0.2 μM ABA was insufficient to effectively suppress seed germination.

Drought-stress tolerance

To assess drought tolerance, the seedlings were transferred to plastic pots, grown for 3 weeks under short-day conditions, and then subjected to drought conditions by withholding water from the plants for 20 days. The drought-induced phenotypes were photographed with a camera. The survival rates of each genotype were analysed at 2 days after rewetting.

Stomatal aperture measurements

For the stomatal aperture assay, leaves were collected from 5-week-old plants and incubated in MES buffer (10 mM MES-KOH (pH 6.15), 10 mM KCl, and 50 μM CaCl₂) under light for 3 h at 23 °C to open the stomata. To examine ABA-induced stomatal closure, 20 μM ABA was added to the MES buffer, which was subsequently incubated for an additional 2 h under the same conditions. In each individual sample, at least 80 stomata were randomly observed, and images were obtained with a microscope. The stomatal aperture was measured using ImageJ software.

Measurement of water loss

Three-week-old seedlings grown under short-day conditions (16-h light/8-h dark) were used for water loss measurements. The whole rosettes were cut from the plants and weighed at the indicated points.

Ion leakage assay

Ion leakage induced by cell death was analysed as previously described⁵⁴. In brief, three 9-mm leaf discs were rinsed three times with distilled water and then soaked in 9 mL distilled water for 3 h at room temperature. The conductivity of the solution was measured using a conductivity meter to generate S1. The leaf discs were then boiled for 20 min, after which the conductivity was measured again to determine

the value of S2. Electrolyte leakage was calculated as the percentage (%) of "S1"/"S2". The assay was repeated three times.

Immunoblot assay

To extract proteins from plant materials, leaves were frozen in liquid nitrogen and ground to a fine powder. Extraction buffer (50 mM HEPES, 150 mM KCl, 1 mM EDTA, and 0.1% [v/v] Triton X-100; pH 7.5) containing 1 mM DTT and protease inhibitor cocktail (Sigma) was used for protein extraction. Anti-GFP antibody (1:5000; #M20004; Abmart) and HRP-conjugated anti-mouse IgG (1:10,000, Sigma-Aldrich) secondary antibody were used for immunoblotting protein with a GFP tag. mAb-HRP-DirecT anti-FLAG antibody (1:5000; #M185-7; MBL) was used for immunoblotting proteins with a FLAG tag. mAb-HRP-DirecT anti-HA antibody (1:5000; #M180-7; MBL) was used for immunoblotting proteins with an HA tag.

Yeast two-hybrid assay

To detect the interaction between FL7 and PP2C-As, the cDNA fragments of FL7 and PP2C-As were amplified by PCR and cloned and inserted into the pGBKT7 and pGADT7 vectors, respectively. The bait and prey constructs were cotransformed into the yeast strain AH109. Successfully transformed colonies were selected on yeast SD medium lacking Trp and Leu. Transformants were subsequently transferred to selective SD medium lacking Trp, Leu, and His for growth analysis. Photographs were taken after 4 days of incubation at 30 °C.

Co-IP assay

Arabidopsis protoplasts were transfected with the indicated plasmid combinations and control constructs, and transfection was performed as described above. Immunoprecipitation with anti-FLAG antibodies was carried out as previously described⁵⁵. Total protein and immunoprecipitates were separated by SDS-PAGE and detected by immunoblotting.

Protein purification

Proteins with different tags were expressed in Rosetta (DE3) *Escherichia coli* cells growing in LB medium supplemented with 0.5 mM IPTG for 18 h at 18 °C. The culture was then collected by centrifugation at 6000 × g for 10 min at 4 °C. For His-tagged proteins, the pellet was resuspended in lysis buffer (50 mM NaH₂PO₄, 30 mM NaCl, 10 mM imidazole (pH 8.0), 1 mM PMSF, and protease inhibitor cocktail (Abmart, A10004)) and then sonicated for 10 min. After centrifugation for 30 min at 7000 g and 4 °C, the supernatant was incubated with Ni Sepharose (GE) resin for 3 h at 4 °C. The resin was subsequently washed three times with washing buffer (50 mM NaH₂PO₄, 30 mM NaCl, and 50 mM imidazole; pH 8.0) to remove nonspecifically bound proteins. The His-tagged proteins were eluted from the resin with elution buffer (50 mM NaH₂PO₄, 30 mM NaCl, and 250 mM imidazole, pH 7.4). For the GST-tagged proteins, the pellet was resuspended in phosphate-buffered saline (PBS) (150 mM NaCl, 10 mM Na₂HPO₄, 2 mM KH₂PO₄, 2.7 mM KCl (pH 7.4), 1 mM PMSF, and inhibitor cocktail) and then sonicated for 10 min. After centrifugation for 30 min at 7000 g and 4 °C, the supernatant was incubated with glutathione Sepharose 4B (GE) resin for 3 h at 4 °C. The resin was subsequently washed three times with PBS to remove nonspecifically bound proteins. The GST-tagged proteins were eluted from the resin with GSH buffer (50 mM Tris-HCl, pH 8.0, and 10 mM GSH). For MBP-tagged proteins, the pellet was resuspended in lysis buffer (20 mM Tris-HCl (pH 7.4), 200 mM NaCl, 1 mM EDTA, 1 mM PMSF, and inhibitor cocktail) and then sonicated for 10 min. After centrifugation for 30 min at 7000 g and 4 °C, the supernatant was incubated with amylose resin (NEB) for 3 h at 4 °C. The resin was subsequently washed three times with lysis buffer to remove nonspecifically bound proteins. The MBP-tagged proteins were eluted from the resin with elution buffer (20 mM Tris-HCl (pH 7.4), 200 mM NaCl, 1 mM EDTA, and 10 mM maltose). To

measure their concentrations, the purified proteins were mixed with Quick Start Bradford Dye Reagent (Bio-Rad), and the absorbance was measured at 595 nm. Protein concentrations were calculated on the basis of a standard curve with bovine serum albumin (BSA) as a substrate.

Protein pull-down assay

The coding sequences of the genes of interest were subsequently cloned and inserted into the MBP vector or the pGEX-6P vector. Recombinant MBP-PP2C, GST, and GST-FL7 proteins were purified as described above. Purified GST or GST-FL7 (10 mg) in 2 mL of lysis buffer (150 mM NaCl, 10 mM Na₂HPO₄, 2 mM KH₂PO₄, 2.7 mM KCl (pH 7.4), 1 mM PMSF, and inhibitor cocktail) was incubated with glutathione beads for 2 h at 4 °C. After a brief centrifugation at 1000 × g for 3 min at 4 °C, the buffer was removed, and 2 mg of recombinant MBP-PP2C protein was added to the resin in 2 mL of lysis buffer. The tube was rotated at 4 °C for 2 h for protein binding. The resin was then washed five times with PBS to remove nonspecifically bound protein, resuspended in 50 mL of PBS and 10 mL of SDS loading buffer, and boiled for 5 min. After centrifugation at 12,000 × g for 1 min at 22 °C, the supernatant was subjected to immunoblotting analysis. Immunoblot assays were conducted with anti-GST (1:5000; #M20007; Abmart) or anti-MBP (1:5000; #M20001; Abmart) antibodies and HRP-conjugated anti-mouse IgG (1:10,000; Sigma-Aldrich) as the secondary antibody.

MST assay

The interactions between ABA and recombinant GST-FL7, GST-PYL10, and GST were measured by MST (microscale thermophoresis). MST assays were performed as previously described⁵⁶.

First, the purified GST, GST-FL7, and GST-PYL10 sample proteins were exchanged for buffer with labelling buffer (130 mM NaHCO₃, 50 mM NaCl, pH 8.2–8.3) and then labelled with dye in assay buffer using the Protein Labelling Kit RED-NHS 2nd Generation (Cat# MO-L011). ABA at a range of concentrations (0.3 µM to 10 mM) was incubated with 2.5 µM labelled protein for 30 min at room temperature, after which the samples were loaded onto NanoTemper glass capillaries (NanoTemper Technologies), and MST was performed. The experimental data were processed, and the Kd values for ABA-FL7, ABA-PYL10, and ABA-GST binding were calculated through MO. Affinity Analysis software.

In vitro dephosphorylation of MAPK

The *Escherichia coli* strain Rosetta (DE3) was used for the production of recombinant proteins. To prepare phosphorylated MAPK, 5 µg of recombinant purified MBP-tagged kinase-inactive MAPK was incubated with 1 µg of GSTMKK4DD at 30 °C for 1 h in kinase buffer (25 mM Tris-HCl (pH 7.5), 1 mM DTT, 10 mM MgCl₂, and 200 µM ATP). The kinase reaction was terminated by removing ATP from the reaction using an Amicon Ultra30K centrifugation unit (Millipore). To test the phosphatase activity of ABI1, phosphorylated MAPK (500 ng) was incubated with MBP or MBP-ABI1 (2 µg) at 30 °C for 15 min in phosphatase buffer (25 mM Tris-HCl (pH 7.5), 1 mM DTT, and 10 mM MgCl₂). MAPK was detected by immunoblotting as described above. To test whether FL7 inhibits the phosphatase activity of ABI1, phosphorylated MAPK (500 ng) and MBP-ABI1 (2 µg) were incubated with GST or GST-FL7 at 30 °C for 15 min in phosphatase buffer (25 mM Tris-HCl (pH 7.5), 1 mM DTT, and 10 mM MgCl₂).

Measurement of PP2C-A activity

In vitro PP2C-A activity was measured using a Ser/Thr Phosphatase Assay Kit (Promega, V2460). In brief, the recombinant proteins were purified with buffers that did not contain phosphate. To measure phosphatase activity, different combinations of recombinant purified FL7 and PP2Cs were mixed with 5 mL of 1 mM phosphopeptide and

10 mL of PP2C reaction buffer (250 mM imidazole (pH 7.2), 1 mM EGTA, 25 mM MgCl₂, 0.1% [v/v] β-mercaptoethanol, and 0.5 mg/mL BSA) in the wells of a microtiter dish and then incubated at 25 °C for 15 min. The reactions were stopped by the addition of 50 mL of molybdate dye/additive mixture, after which the plate was incubated at room temperature for 15 min. The absorbance was measured at 630 nm in a microplate reader (Molecular Devices, SpectraMax M5). Michaelis–Menten plots in GraphPad Prism 9.0 were used to calculate the kinetic parameters.

To measure PP2C activity *in vivo*, total proteins (0.1 g) from the wild type or *f17*, *OE-F17*, or *OE-F17N* mutants were extracted using phosphatase storage buffer (20 mM Tris–HCl (pH 7.5), 20 mM KCl, 1 mM EDTA, 1 mM EGTA, 10 mM DTT, 0.5% [v/v] Triton X-100, and 50% [v/v] glycerol) with a protease inhibitor cocktail (Abmart, A10004), after which the homogenised lysate was centrifuged at 100,000 × g for 1 h at 4 °C. The supernatant was filtered through Sephadex G-25 resin to remove endogenous phosphates, after which the lysate was used to measure PP2C activity as described above, but 5 mM okadaic acid was added to inhibit the activity of PP1 and PP2A family Ser/Thr-specific phosphoprotein phosphatases²⁵.

In vitro kinase assays

The recombinant protein was expressed in Rosetta (DE3) and affinity purified according to the instructions described above. Two micrograms of GST or GST-F17 proteins were incubated with 0.5 μg of MBP-ABI1 with or without 0.5 μM ABA in 20 μL of phosphatase buffer (50 mM Tris-HCl (pH 7.5), 10 mM MgCl₂, 1 mM EGTA and 0.1% [v/v] β-mercaptoethanol). After 15 min of incubation, 1 μg of SnRK2.6-HIS protein was added to the reaction buffer and incubated for another 15 min. Then, the reaction buffer was mixed with 1 μM ATP and phosphatase inhibitor cocktail 3 to a total volume of 25 μL and incubated for 30 min at 25 °C. The reactions were stopped by the addition of SDS loading buffer, and the mixtures were separated by SDS-PAGE. The anti-phospho-S175-SnRK2 antibody was previously reported (1:5000)³². The protein level was analysed by Coomassie Brilliant Blue (CBB) staining.

SnRK2.6 kinase activity *in vivo*

To assess the kinase activity of SnRK2.6 *in vivo*, total protein was extracted from Col-0, *f17* and *OE-F17* with lysis buffer (100 mM HEPES (pH 7.8), 10 mM Na₃VO₄, 10 mM NaF, 5 mM EDTA, 5 mM EGTA, 10 mM DTT, 1 mM PMSF, and 5% glycerin and protease inhibitor cocktail), separated by SDS-PAGE and detected by immunoblotting with anti-phosphorylation antibodies against Ser175 in SnRK2.6³⁵.

Arabidopsis protoplast preparation and transfection

Fully expanded rosette leaves from 4-week-old Col-0 plants were enzymatically digested to release protoplasts⁵⁵, which were washed and resuspended at $\sim 2 \times 10^6$ cells/ml. For each transfection, 100 μl protoplasts ($\sim 2 \times 10^5$ cells) were mixed with 20 μg plasmid DNA and an equal volume of PEG solution (40% PEG4000, 0.2 M mannitol, 100 mM CaCl₂), incubated 10–15 min, then diluted with W5 (154 mM NaCl, 125 mM CaCl₂, 5 mM KCl, and 2 mM MES; pH 5.7) and recovered. Transfected protoplasts were incubated in the dark at 22 °C for 12–24 h before downstream assays.

Phylogenetic analysis

Multiple alignments of full-length aa sequences were aligned using MUSCLE. Phylogenetic analysis was performed using full-length sequences with the MEGA X program by the maximum-likelihood method with 100 bootstrap samples and the following parameters: Poisson model, uniform rates, and complete deletion.

RNA-seq analysis

For RNA sequencing, total RNA from nine-day-old seedlings treated with or without 300 mM mannitol on 1/2 MS solid medium for 12 h³⁵

was extracted using an RNA-Simple Total RNA Kit (Zoman Biotech) and prepared for RNA sequencing at Novogene (Beijing, China). The sequencing data were initially filtered, after which the clean reads were mapped to the *Arabidopsis* genome using HISAT2⁵⁷. The transcripts per million (TPM) value of each gene was quantified using the Stringtie tool⁵⁸. DEGSeq2 facilitated the identification of differentially expressed genes (DEGs) across samples, focusing on genes that exhibited a $|\log_2(\text{fold change})| \geq 1$ and a $P \leq 0.05$ as DEGs⁵⁸. Gene expression patterns were clustered using the pheatmap package in R, employing the ward.D2 clustering algorithm. GO enrichment analyses were conducted with the GO.db package in R.

Statistical analysis

All data are shown as the means \pm standard deviations (SD) from at least three biological replicates or from three technical replicates in one of three experiments with similar results. Two-tailed Student's *t* test was used to compare the means between two samples (* and ** represent $P < 0.05$ and 0.01, respectively). One- or two-way analysis of variance (ANOVA) was used to test the significance of the difference among different group means (different lowercase letters indicate significant differences; $P < 0.05$). Detailed statistical reports are provided in the source data for the figures.

Accession numbers

Sequence data from this article can be found in the TAIR (The *Arabidopsis* Information Resource) databases under the following accession numbers: F17 (At4g16670), ABI1 (At4g26080), ABI2 (At5g57050), HAB1 (At1g72770), HAB2 (At1g17550), HAI1 (At5g59220), HAI2 (At1g07430), HAI3 (At2g29380), AHG1 (At5g51760), AHG3 (At3g11410), PP2C-D (At5g02760), PYL10 (At4g27920), SnRK2.6 (At4g33950), MPK6 (At2g43790), MKK4 (At1g51660), RD29B (At5g52300), AFP1 (At1g69260), AtNAP (At1g69490), P5CS1 (At2g39800), SAG13 (At2g29350), ABF2 (At1g45249), COR413IM1 (At1g29395), EGY3 (At1g17870), GOLS2 (At1g56600), LEA7 (At1g52690), PNP-A (At2g18660), RAB18 (At5g66400), SINA2 (At3g13672) and ABA1 (At5g67030).

Reporting summary

Further information on research design is available in the Nature Portfolio Reporting Summary linked to this article.

Data availability

Source data and uncropped western blot membranes are provided with this paper. The RNA-seq raw read data generated in this study have been deposited in the National Genomics Data Center database under accession code [CRA020685](#). Source data are provided with this paper.

References

1. Kim, J. H., Hilleary, R., Seroka, A. & He, S. Y. Crops of the future: building a climate-resilient plant immune system. *Curr. Opin. Plant Biol.* **60**, 101997 (2021).
2. van Zelm, E., Zhang, Y. X. & Testerink, C. Salt tolerance mechanisms of plants. *Annu. Rev. Plant Biol.* **71**, 403–433 (2020).
3. Shoaib, A., Meraj, S., Nafisa, Khan, K. A. & Javaid, M. A. Influence of salinity and as the stress factors on morphophysiological and yield attributes in onion. *Physiol. Mol. Biol. Plants* **24**, 1093–1101 (2018).
4. Dileo, M. V. et al. Abscisic acid in salt stress predisposition to phytophthora root and crown rot in tomato and chrysanthemum. *Phytopathology* **100**, 871–879 (2010).
5. Kusajima, M. et al. Suppressive effect of abscisic acid on systemic acquired resistance in tobacco plants. *J. Gen. Plant Pathol.* **76**, 161–167 (2010).

6. Yasuda, M. et al. Antagonistic interaction between systemic acquired resistance and the abscisic acid-mediated abiotic stress response in *Arabidopsis*. *Plant Cell* **20**, 1678–1692 (2008).
7. Audenaert, K., De Meyer, G. B. & Hofte, M. M. Abscisic acid determines basal susceptibility of tomato to *Botrytis cinerea* and suppresses salicylic acid-dependent signaling mechanisms. *Plant Physiol.* **128**, 491–501 (2002).
8. Ulferts, S., Delventhal, R., Splivallo, R., Karlovsky, P. & Schaffrath, U. Abscisic acid negatively interferes with basal defence of barley against *Magnaporthe oryzae*. *BMC Plant Biol.* **15**, 7 (2015).
9. Zhang, H., Zhao, Y. & Zhu, J. K. Thriving under stress: how plants balance growth and the stress response. *Dev. Cell* **55**, 529–543 (2020).
10. Bhaskara, G. B., Wong, M. M. & Verslues, P. E. The flip side of phospho-signalling: regulation of protein dephosphorylation and the protein phosphatase 2Cs. *Plant Cell Environ.* **42**, 2913–2930 (2019).
11. Schweighofer, A., Hirt, H. & Meskiene, L. Plant PP2C phosphatases: emerging functions in stress signaling. *Trends Plant Sci.* **9**, 236–243 (2004).
12. Tischer, S. V. et al. Combinatorial interaction network of abscisic acid receptors and coreceptors from *Arabidopsis thaliana*. *Proc. Natl. Acad. Sci. USA* **114**, 10280–10285 (2017).
13. Zhu, J. K. Abiotic stress signaling and responses in plants. *Cell* **167**, 313–324 (2016).
14. Bhaskara, G. B., Nguyen, T. T. & Verslues, P. E. Unique drought resistance functions of the highly ABA-induced clade A protein phosphatase 2Cs. *Plant Physiol.* **160**, 379–395 (2012).
15. Rubio, S. et al. Triple loss of function of protein phosphatases type 2C leads to partial constitutive response to endogenous abscisic acid. *Plant Physiol.* **150**, 1345–1355 (2009).
16. Mine, A. et al. Pathogen exploitation of an abscisic acid- and jasmonate-inducible MAPK phosphatase and its interception by *Arabidopsis* immunity. *Proc. Natl. Acad. Sci. USA* **114**, 7456–7461 (2017).
17. Leung, J. et al. Antagonistic interaction between MAP kinase and protein phosphatase 2C in stress recovery. *Plant Sci.* **171**, 596–606 (2006).
18. Shi, Y. G. Serine/Threonine phosphatases: mechanism through structure. *Cell* **139**, 468–484 (2009).
19. Lillo, C. et al. Protein phosphatases PP2A, PP4 and PP6: mediators and regulators in development and responses to environmental cues. *Plant Cell Environ.* **37**, 2631–2648 (2014).
20. Soon, F. F. et al. Molecular mimicry regulates ABA signaling by SnRK2 kinases and PP2C phosphatases. *Science* **335**, 85–88 (2012).
21. Chen, K. et al. Abscisic acid dynamics, signaling, and functions in plants. *J. Integr. Plant Biol.* **62**, 25–54 (2020).
22. Park, S. Y. et al. Abscisic acid inhibits type 2C protein phosphatases via the PYR/PYL Family of START Proteins. *Science* **324**, 1068–1071 (2009).
23. Fujii, H. et al. In vitro reconstitution of an abscisic acid signalling pathway. *Nature* **462**, 660–U138 (2009).
24. Hao, Q. et al. The molecular basis of ABA-independent inhibition of PP2Cs by a subclass of PYL proteins. *Mol. Cell* **42**, 662–672 (2011).
25. Wang, K. et al. EAR1 negatively regulates ABA signaling by enhancing 2C protein phosphatase activity. *Plant Cell* **30**, 815–834 (2018).
26. Li, Z. et al. ROP11 GTPase negatively regulates ABA signaling by protecting ABI1 phosphatase activity from inhibition by the ABA receptor RCAR1/PYL9 in *Arabidopsis*. *J. Integr. Plant Biol.* **54**, 180–188 (2012).
27. Yu, F. et al. FERONIA receptor kinase pathway suppresses abscisic acid signaling in *Arabidopsis* by activating ABI2 phosphatase. *Proc. Natl. Acad. Sci. USA* **109**, 14693–14698 (2012).
28. Baek, W., Lim, C. W. & Lee, S. C. A DEAD-box RNA helicase, RH8, is critical for regulation of ABA signalling and the drought stress response via inhibition of PP2CA activity. *Plant Cell Environ.* **41**, 1593–1604 (2018).
29. Nishimura, N. et al. Control of seed dormancy and germination by DOG1-AHG1 PP2C phosphatase complex via binding to heme. *Nat. Commun.* **9**, 2132 (2018).
30. Prabhakaran Mariyamma, N. et al. Members of the *Arabidopsis* FORKED1-LIKE gene family act to localize PIN1 in developing veins. *J. Exp. Bot.* **69**, 4773–4790 (2018).
31. Hou, H. W., Erickson, J., Meservy, J. & Schultz, E. A. FORKED1 encodes a PH domain protein that is required for PIN1 localization in developing leaf veins. *Plant J.* **63**, 960–973 (2010).
32. Zeng, D., Lv, J., Li, X. & Liu, H. The *Arabidopsis* blue-light photoreceptor CRY2 is active in darkness to inhibit root growth. *Cell*, <https://doi.org/10.1016/j.cell.2024.10.031> (2024).
33. Ai, G. et al. BPL3 binds the long non-coding RNA nalncFL7 to suppress FORKED-LIKE7 and modulate HA11-mediated MPK3/6 dephosphorylation in plant immunity. *Plant Cell* **35**, 598–616 (2023).
34. Yu, B., Chao, D. Y. & Zhao, Y. How plants sense and respond to osmotic stress. *J. Integr. Plant Biol.* **66**, 394–423 (2024).
35. Chen, K. et al. BONZAI proteins control global osmotic stress responses in plants. *Curr. Biol.* **30**, 4815–4825.e4814 (2020).
36. Blat, Y. Non-competitive inhibition by active site binders. *Chem. Biol. Drug Des.* **75**, 535–540 (2010).
37. Ye, Y. J. et al. A novel chemical inhibitor of ABA signaling targets all ABA receptors. *Plant Physiol.* **173**, 2356–2369 (2017).
38. de Vries, J., Curtis, B. A., Gould, S. B. & Archibald, J. M. Embryophyte stress signaling evolved in the algal progenitors of land plants. *Proc. Natl. Acad. Sci. USA* **115**, E3471–E3480 (2018).
39. Cheng, S. F. et al. Genomes of Subaerial Zygnematophyceae Provide Insights into Land Plant Evolution. *Cell* **179**, 1057 (2019).
40. Bierendorfspot, M. J. et al. Phylogenomic insights into the first multicellular streptophyte. *Curr. Biol.* **34**, <https://doi.org/10.1016/j.cub.2023.12.070> (2024).
41. Timme, R. E., Bachvaroff, T. R. & Delwiche, C. F. Broad phylogenomic sampling and the sister lineage of land plants. *Plos ONE* **7**, e29696 (2012).
42. Ju, C. et al. Conservation of ethylene as a plant hormone over 450 million years of evolution. *Nat. Plants* **1**, 14004 (2015).
43. Wang, C., Liu, Y., Li, S. S. & Han, G. Z. Insights into the origin and evolution of the plant hormone signaling machinery. *Plant Physiol.* **167**, 872–886 (2015).
44. Sun, Y. et al. A ligand-independent origin of abscisic acid perception. *Proc. Natl. Acad. Sci. USA* **116**, 24892–24899 (2019).
45. Fuchs, S., Grill, E., Meskiene, I. & Schweighofer, A. Type 2C protein phosphatases in plants. *FEBS J.* **280**, 681–693 (2013).
46. Yoshida, T., Mogami, J. & Yamaguchi-Shinozaki, K. ABA-dependent and ABA-independent signaling in response to osmotic stress in plants. *Curr. Opin. plant Biol.* **21**, 133–139 (2014).
47. Nishimura, N. et al. ABA-Hypersensitive Germination1 encodes a protein phosphatase 2C, an essential component of abscisic acid signaling in *Arabidopsis* seed. *Plant J.* **50**, 935–949 (2007).
48. Nee, G. et al. DELAY OF GERMINATION1 requires PP2C phosphatases of the ABA signalling pathway to control seed dormancy. *Nat. Commun.* **8**, 72 (2017).
49. Komatsu, K., Takezawa, D. & Sakata, Y. Decoding ABA and osmotic stress signalling in plants from an evolutionary point of view. *Plant Cell Environ.* **43**, 2894–2911 (2020).
50. Lind, C. et al. Stomatal guard cells co-opted an ancient ABA-dependent desiccation survival system to regulate stomatal closure. *Curr. Biol.* **25**, 928–935 (2015).
51. Shinozawa, A. et al. SnRK2 protein kinases represent an ancient system in plants for adaptation to a terrestrial environment. *Commun. Biol.* **2**, 30 (2019).

52. Zhao, Y. et al. Arabidopsis Duodecuple mMutant of PYL ABA receptors reveals PYL repression of ABA-independent SnRK2 activity. *Cell Rep.* **23**, 3340 (2018).
53. Yuan, X. P. & Zhao, Y. SnRK2 kinases sense molecular crowding and form condensates to disrupt ABI1 inhibition. *Sci. Adv.* **11**, eadr8250 (2025).
54. Ai, G. et al. A CRN effector mediates phosphorylation and degradation of plant aquaporin proteins to suppress host immune signaling. *Plos Pathogens* **17**, ARTN e1009388, <https://doi.org/10.1371/journal.ppat.1009388> (2021).
55. Zhu, H. et al. Phosphorylation of PIP2;7 by CPK28 or Phytophthora kinase effectors dampens pattern-triggered immunity in Arabidopsis. *Plant Commun.* 101135, <https://doi.org/10.1016/j.xplc.2024.101135> (2024).
56. Wang, P. et al. Reciprocal regulation of the TOR Kinase and ABA receptor balances plant growth and stress response. *Mol. Cell* **69**, 100–112.e106 (2018).
57. Pertea, M., Kim, D., Pertea, G. M., Leek, J. T. & Salzberg, S. L. Transcript-level expression analysis of RNA-seq experiments with HISAT, StringTie and Ballgown. *Nat. Protoc.* **11**, 1650–1667 (2016).
58. Love, M. I., Huber, W. & Anders, S. Moderated estimation of fold change and dispersion for RNA-seq data with DESeq2. *Genome Biol.* **15**, 550 (2014).

Acknowledgements

The anti-phosphorylation antibodies for Ser175 in SnRK2.6 is a gift from Y.Z. in CAS Center for Excellence in Molecular Plant Sciences, China. We thank Pro. Assaf Mosquna in the Hebrew University of Jerusalem, Israel, and Pro. Yajin Ye in Nanjing Forestry University, China for helpful suggestions and for manuscript editing. The work was supported by the Natural Science Foundation of Jiangsu Province, China (BK20230984, G.A.), the National Natural Science Foundation of China (32402315, G.A.; 32230089, D.D.; 32372493, D.S.), the China Agriculture Research System (CARS-21, D.D.) and the National Key Research and Development Program (2024YFD1401103, G.A.).

Author contributions

G.A., D.S., and D.D. conceived and designed the project. T.L., Z.Y., G.L., Y.L., X.Li., X.Lu., X.G., and Z.C. performed experiments and analyzed data. D.S., J.d.V., Y.Z., G.A., and D.D. wrote the manuscript. All authors reviewed and approved the final manuscript.

Competing interests

The authors declare no competing interests.

Additional information

Supplementary information The online version contains supplementary material available at <https://doi.org/10.1038/s41467-025-66086-z>.

Correspondence and requests for materials should be addressed to Danyu Shen or Gan Ai.

Peer review information *Nature Communications* thanks Yoichi Sakata, and Cun Wang for their contribution to the peer review of this work. A peer review file is available.

Reprints and permissions information is available at <http://www.nature.com/reprints>

Publisher's note Springer Nature remains neutral with regard to jurisdictional claims in published maps and institutional affiliations.

Open Access This article is licensed under a Creative Commons Attribution-NonCommercial-NoDerivatives 4.0 International License, which permits any non-commercial use, sharing, distribution and reproduction in any medium or format, as long as you give appropriate credit to the original author(s) and the source, provide a link to the Creative Commons licence, and indicate if you modified the licensed material. You do not have permission under this licence to share adapted material derived from this article or parts of it. The images or other third party material in this article are included in the article's Creative Commons licence, unless indicated otherwise in a credit line to the material. If material is not included in the article's Creative Commons licence and your intended use is not permitted by statutory regulation or exceeds the permitted use, you will need to obtain permission directly from the copyright holder. To view a copy of this licence, visit <http://creativecommons.org/licenses/by-nc-nd/4.0/>.

© The Author(s) 2025